

Local density approximation for excited states

Tim Gould

Queensland Micro- and Nanotechnology Centre, Griffith University, Nathan, Qld 4111, Australia*

Stefano Pittalis

CNR-Istituto Nanoscienze, Via Campi 213A, I-41125 Modena, Italy

The ground state of an homogeneous electron gas is a paradigmatic state that has been used to model and predict the electronic structure of matter at equilibrium for nearly a century. For half a century, it has been successfully used to predict ground states of quantum systems via the local density approximation (LDA) of density functional theory (DFT); and systematic improvements in the form of generalized gradient approximations and evolution thereon. Here, we introduce the LDA for *excited* states by considering a particular class of non-thermal ensemble states of the homogeneous electron gas. These states find sound foundation and application in ensemble-DFT – a generalization of DFT that can deal with ground and excited states on equal footing. The ensemble-LDA is shown to successfully predict difficult low-lying excitations in atoms and molecules for which approximations based on local spin density approximation (LSDA) and time-dependent-LDA fail.

I. INTRODUCTION

Excitation of many-electron systems characterize novel states of matter and increasingly permeate the functions of novel advanced technologies. In problems ranging from photovoltaic devices to quantum dots to nano-particle catalysts to quantum computing devices, particle-like, collective, or topological excitations are exploited coherently. Challenges are multidisciplinary, yet solutions can be inspired – and, increasingly, predicted – by computationally investigating quantum structures and mechanisms at the nanoscale. Density functional theory [1, 2] (DFT) has dominated the stage of computational electronic structure methodologies since the 1960s, by balancing accuracy with efficiency. But DFT does not handle excited states directly, being restricted to addressing eigenstates of lowest energy (i.e. ground states). This work will show how successful DFT methods for ground states can be upgraded into methods for *also* tackling excited states.

The most fundamental model from which DFT gained inspiration, can be traced back to the seminal works by Thomas and Fermi [3, 4]. In 1927, they independently proposed a remarkable approximation for quantum physics – that the state of any many-electron system can be modelled by referring, via the particle density (a local quantity), to an homogenous gas of electrons. Due to its poor treatment of kinetic energy contributions, the resulting Thomas-Fermi approximation is not very good in practice. But almost all modern modelling of electronic structure employs its spiritual descendent, in the form of Kohn-Sham DFT [1, 2]: 1) kinetic energy contributions are treated quantum mechanically, via a non-interacting auxilliary system; 2) the energy of electrostatic interactions is treated classically, for any given particle density; 3) the HEG is *only* used to treat the re-

maining quantum exchange-correlation (xc) energy contributions.

The homogeneous electron gas (HEG [5]) is, arguably, the simplest many-electron system. It involves $N \rightarrow \infty$ electrons interacting in response to a uniform positive background charge of fixed density, n , and volume, $V = N/n \rightarrow \infty$. The resulting (interacting) electronic structure problem can be solved semi-analytically in its high-density and low-density limits, and to high accuracy for moderate densities using quantum Monte Carlo (QMC) techniques. [6–8] The *known* paradigmatic xc behaviour of HEG may then be used to approximate the *unknown* xc behaviour of inhomogeneous quantum systems, via parametrisations. [9–11]. Crucially, it has also been recognised that the LDA provides exact leading terms in a semi-classical expansion of any quantum system, under appropriate limits; [12–14] which helps to explain the ongoing success of the Jacob’s ladder [15] philosophy of systematically improving on the LDA. [16–19]

What about excited states? In the late 1980s, the time-dependent extension of DFT (TDDFT) was revealed to be an highly effective tool for simulating spectra, via a perturbative (linear-response) expansion around the ground state. But, despite its ongoing success, it was soon revealed [20, 21] that approximations to TDDFT could not describe important double excitations at all; and struggle to describe charge transfer excitations except by using specialized approximations. [22–24] More recently, singlet-triplet inversion [25] (with great promise for photovoltaics) has emerged as another important problem where TDDFT struggles. [26, 27]

In parallel with TDDFT, Kohn and collaborators put forward a density functional theory for *stationary* excitations based on mixed states (ensembles) rather than pure states: ensemble-DFT (EDFT). [28, 29] Unlike the perturbation-based formalism of TDDFT, EDFT recast the problem of computing excited states into an extended “ground state”-like problem involving variational minima. TDDFT’s rapid success in predicting spectra,

* t.gould@griffith.edu.au

and challenges in constructing useful ensemble approximations, initially led to EDFT falling by the wayside. Recently, however, it has re-emerged as a powerful alternative to TDDFT because approximations in EDFT can solve precisely those excitation problems for which TDDFT struggles or fails. [30–42]

Moreover, recent theoretical breakthroughs [35, 43–47] have revealed aspects of the architecture of key functional forms in EDFT that have opened unprecedented possibilities for novel approximations for excited states. The change of perspective brought about by EDFT compared to (TD)DFT is radical: 1) the auxiliary states of the Kohn-Sham ensemble can acquire the form of coherent (finite) superposition of Slater determinants (rather than the ‘disentangled’ single determinant for pure ground states); 2) the ensemble Hartree energy (in contrast to the *classical* Hartree energy) accounts for peculiar quantum features; 3) the ensemble exchange energy does not (necessarily) reduce to textbook Fock-exchange expressions; 4) in addition to regular-looking state-driven correlations, unusual density-driven correlations emerge.

In this work, we demonstrate that the same system of knowledge allows us to derive an exchange-correlation energy approximation from first principles (*ab initio*). We consider the prominent example of approximations that are derivable from the HEG. Given nearly 100 years of exploration, one might expect the HEG to have given up all its useful secrets. Crucially this work reveals that when the HEG is viewed from the perspective of EDFT, we can introduce a class of non-thermal ensembles from which we can derive a local approximation for excited states *directly*. The regular LDA has provided an highly-effective cornerstone for systematic improvements for ground states – both as the first rung of Jacob’s ladder [15] and as a paradigmatic/semi-classical limit that can constrain functional forms [16–18, 48]. The ensemble-LDA developed in this work therefore provides us with a (long-sought) cornerstone for systematic improvements to approximations for excited states.

The remainder of this work is organized as follows: Section II gives an introduction to the HEG in the context of density functional theory, and briefly introduce the elements of ensemble-DFT which are exploited in the novel parts of the work. Section III presents the relevant ensemble-states of HEG, which are designed to capture excited-state physics in crucial energy components of the HEG ensemble-states (Appendix D reports a parametrisation). Section IV demonstrates the practical usefulness of the formal developments done by setting up and applying an ensemble-LDA to atoms and molecules. Finally, Section V summarizes the work, looks toward the near future, and draws conclusions.

II. THEORETICAL BACKGROUND

The properties of HEGs are conventionally defined using the the Wigner-Seitz radius, $r_s := (\frac{3}{4\pi n})^{1/3} \approx$

$0.620350n^{-1/3}$, and spin-polarization factor, $\zeta = \frac{n_\uparrow - n_\downarrow}{n}$. Here, n is the density of electrons and $n_{\uparrow,\downarrow}$ are the densities of \uparrow, \downarrow electrons obeying $n_\uparrow + n_\downarrow = n$. This combination of terms reflects the fact that interactions between same- and different-spin electrons are fundamentally different due to the Pauli exclusion principle, so energies change not only with the total density but also the relative contributions of majority (\uparrow) and minority (\downarrow) electrons to the density.

This section will first motivate the standard approach to understanding HEGs, in the context of density functional theory. Then, it introduce ensemble density functional theory, which provides the key theoretical tool for the rest of the work. Throughout, we use atomic units so that lengths (e.g. r_s) are expressed in Bohr and energies (e.g. ϵ_x) are expressed in Hartree (Ha).

A. Understanding HEGs through density functional theory

Density functional theory (DFT) provides an important tool for the analysis and parametrisation of HEGs. Key theorems [1, 49, 50] demonstrate that all properties of a quantum mechanical ground state are described by its density, $n(\mathbf{r})$ (constant, n in an HEG). This is easily extended to spin-DFT, [51] which covers *de facto* ground states like the lowest energy with a given spin-polarization, $\zeta(\mathbf{r})$ (constant ζ in an HEG). DFT is typically used synonymously with Kohn-Sham (KS) DFT, [2] and we shall adopt this convention throughout.

In Kohn-Sham DFT, the ground state energy of an N -electron system in external (nuclear) potential, $v(\mathbf{r})$, is written as,

$$E_0[n] := T_s[n] + \int n v d\mathbf{r} + E_H[n] + E_x[n] + E_c[n], \quad (1)$$

where $[n]$ indicates a functional of the density, $n(\mathbf{r})$, obeying $\int n d\mathbf{r} = N$. Useful exact energy expressions are known for:

1. The Kohn-Sham kinetic energy functional, $T_s[n]$, that includes kinetic energy effects from a *non-interacting* system with the same density (and spin) – we may write $T_s = \sum_{i\sigma \in \text{occ}} \int \frac{1}{2} |\nabla \phi_{i\sigma}(\mathbf{r})|^2 d\mathbf{r}$ using a set of occupied Kohn-Sham orbitals, $\phi_{i\sigma}(\mathbf{r})$; [2]
2. The Hartree energy functional, $E_H[n] = U[n]$, that includes mean-field electrostatic interactions;
3. The Fock exchange energy functional, $E_x[n] = -\sum_{ii'\sigma \in \text{occ}} U[\phi_{i\sigma} \phi_{i'\sigma}^*]$, that includes corrections for Fermionic exchange based on the same non-interacting system used for T_s .

The *unknown* correlation energy functional, $E_c[n]$, captures classical and quantum contributions that are missed in the other terms.

TABLE I. Summary of Kohn-Sham derived properties of the HEGs considered in this work. Here, $C_s = 1.10495$ and $C_x = 0.458165$. The cases $\zeta = 0$ and $\bar{f} = 2$ correspond to an unpolarized gas; and $\zeta = 1$ and $\bar{f} = 1$ are equivalent.

Type of HEG	Params	t_s	ϵ_x	$\Delta\epsilon_H$
Unpolarized gas	r_s	$\frac{C_s}{r_s^2}$	$\frac{-C_x}{r_s}$	0
Polarized gas	r_s, ζ	$\frac{C_s}{r_s^2} \frac{(1+\zeta)^{5/3} + (1-\zeta)^{5/3}}{2}$	$\frac{-C_x}{r_s} \frac{(1+\zeta)^{4/3} + (1-\zeta)^{4/3}}{2}$	0
Constant occupation factor (cof)	r_s, \bar{f}	$\frac{C_s}{r_s^2} \left[\frac{2}{\bar{f}}\right]^{2/3}$	$\frac{-C_x}{r_s} \left[\frac{2}{\bar{f}}\right]^{1/3}$	$ \epsilon_x \frac{(2-\bar{f})(\bar{f}-1)}{\bar{f}}$

Here we introduced an electrostatic Coulomb integral,

$$U[\rho] = \Re \int \rho(\mathbf{r}) \rho^*(\mathbf{r}') \frac{d\mathbf{r} d\mathbf{r}'}{2|\mathbf{r} - \mathbf{r}'|} \quad (2)$$

that was adapted for complex-valued inputs to accommodate classical (here, in E_H only) and quantum (here, in E_x only) interactions. All functionals are readily extended to spin-polarized ground states by introducing the number, $N_\uparrow \leq N$, of \uparrow electrons ($N_\downarrow = N - N_\uparrow$) as an additional constraint, or equivalently setting $\zeta = \frac{N_\uparrow - N_\downarrow}{N}$. Precise details do not matter at this point and will be introduced as required.

In a standard HEG, the mean-field Hartree contribution (from E_H) is cancelled exactly by the positive background charge. The energy per particle, $e = E/N$, of an HEG may therefore be separated into three components,

$$e(n, \zeta) = t_s(n, \zeta) + \epsilon_x(n, \zeta) + \epsilon_c(n, \zeta), \quad (3)$$

using eq. (1). Here, n and ζ are scalar constants; and $t_s := T_s/N$, $\epsilon_x := E_x/N$ and $\epsilon_c := E_c/N$ are energy densities per particle. The Kohn-Sham kinetic and exchange energies may be obtained analytically, and are,

$$t_s(r_s, \zeta) = t_s(r_s) \frac{(1+\zeta)^{5/3} + (1-\zeta)^{5/3}}{2} := t_s(r_s) f_s(\zeta), \quad (4)$$

$$\epsilon_x(r_s, \zeta) = \epsilon_x(r_s) \frac{(1+\zeta)^{4/3} + (1-\zeta)^{4/3}}{2} := \epsilon_x(r_s) f_x(\zeta), \quad (5)$$

where,

$$t_s(r_s) := \frac{C_t}{r_s^2} = \frac{3}{10} \left(\frac{9\pi}{4}\right)^{2/3} r_s^{-2} = 1.10495 r_s^{-2}, \quad (6)$$

$$\epsilon_x(r_s) := \frac{-C_x}{r_s} = -\frac{3}{4\pi} \left(\frac{9\pi}{4}\right)^{1/3} r_s^{-1} = -0.458165 r_s^{-1}, \quad (7)$$

are the kinetic and exchange energies of an unpolarized HEG (in atomic units). We may alternately write, $t_s(n) = 2.87123 n^{2/3}$ and $\epsilon_x(n) = -0.738559 n^{1/3}$.

The final ingredient is the correlation energy term,

$$\epsilon_c(r_s, \zeta) := \sum_k \epsilon_c^k(r_s) f_c^k(\zeta), \quad (8)$$

which has known series expansions for the high- ($r_s \rightarrow 0$) and low-density ($r_s \rightarrow \infty$) limits, but is unknown in general. Total energies, e^{QMC} , of HEGs may be evaluated to high accuracy via quantum Monte-Carlo (QMC) simulations, which have served to supplement limiting cases since pioneering work by Ceperley and Alder. [6] Then, $\epsilon_c = e^{\text{QMC}} - t_s - \epsilon_x$, may be parametrised (e.g. [9–11])

by a truncated series in the general form of (8). Models and parameters for ϵ_c are usually designed to satisfy or approximately satisfy limiting behaviours of HEGs, with some free parameters that can be optimized to reproduce reference data from QMC at intermediate values.

B. A brief introduction to ensemble DFT

We conclude our theory introduction by digressing from standard DFT text book material, to provide some theoretical foundations for ensemble DFT (EDFT) which addresses a wider class of electronic structure problems than are allowed by conventional DFT. [28, 50, 52–55] The results from this section will then be applied to HEGs, to reveal some surprising results. Specifically, we shall focus on EDFT for excited states [28, 29].

To understand ensemble DFT, let us first define quantum state ensembles. A (quantum state) ensemble, $\hat{\Gamma}$, is an operator that describes a classical mixture of quantum states. It may be defined using a spectral representation,

$$\hat{\Gamma} = \sum_{\kappa} w_{\kappa} |\kappa\rangle \langle \kappa|, \quad 0 \leq w_{\kappa} \leq 1, \quad \sum_{\kappa} w_{\kappa} = 1, \quad (9)$$

in which an arbitrary set of orthonormal quantum states, $|\kappa\rangle$, are assigned probabilities/weights, w_{κ} . Operator expectation values, $\bar{O} = \langle \Psi | \hat{O} | \Psi \rangle$, are replaced by $\bar{O}^w = \text{Tr}[\hat{\Gamma}^w \hat{O}] = \sum_{\kappa} w_{\kappa} \langle \kappa | \hat{O} | \kappa \rangle$ which involves quantum and classical averages. Ensembles are more flexible than wave functions, so can describe constrained, open and degenerate systems that are otherwise outside the remit of wave function mechanics or DFT. Various theorems [28, 29, 54] extend key results of DFT to ensembles, including important variational principles.

In excited state EDFT, the usual variational formula, $E_0 = \min_{\Psi} \langle \Psi | \hat{H} | \Psi \rangle$, is replaced by the weighted average,

$$E^w := \inf_{\hat{\Gamma}^w} \text{Tr}[\hat{\Gamma}^w \hat{H}] = \sum_{\kappa} w_{\kappa} E_{\kappa}, \quad (10)$$

where $\hat{\Gamma}^w$ is an ensemble with a given set of weights $\mathbf{w} = \{w_0, w_1, \dots\}$; and E_{κ} are eigen-energies of \hat{H} ordered such that the lowest energies are associated with the largest weights. The energies are in usual ascending ‘excitation’ order if we define the weights to be monotonically decreasing, i.e. $w_{\kappa'} \leq w_{\kappa}$ for $E_{\kappa'} \geq E_{\kappa}$. Note, we follow the usual convention of using superscripts \mathbf{w}

(or cofe later) to identify ensemble functionals. But we depart from the recent convention of using calligraphic letters to avoid confusion between \mathcal{E} for total energies of ensembles, and ϵ for energies per particle of HEGs.

It is convenient to generalize eq. (1) to ensembles by writing,

$$E^{\mathbf{w}}[n] := T_s^{\mathbf{w}}[n] + \int n v d\mathbf{r} + E_H^{\mathbf{w}}[n] + E_x^{\mathbf{w}}[n] + E_c^{\mathbf{w}}[n]. \quad (11)$$

Here, \mathbf{w} indicates the set of weights, n is the density, and v is the external potential. In a Kohn-Sham formalism, the ensemble density is conveniently written as,

$$n^{\mathbf{w}}(\mathbf{r}) := \sum_k f_k^{\mathbf{w}} n_k(\mathbf{r}), \quad f_k^{\mathbf{w}} := \sum_{\kappa} w_{\kappa} \theta_{\kappa}^{\kappa}, \quad (12)$$

in terms of orbital densities, $n_k(\mathbf{r}) := |\phi_k(\mathbf{r})|^2$; and average occupation factors, $f_k^{\mathbf{w}}$, which may be non-integer and involve a weighted average over the integer occupation factors, $\theta_{\kappa}^{\kappa} \in (0, 1, 2)$ (i.e. no occupation, occupation in one spin, or occupation in both spins) of each KS state in the ensemble. The orbitals obey a spin-independent KS-like equation, $[\hat{t} + v_s^{\mathbf{w}}(\mathbf{r})]\phi_k(\mathbf{r}) = \varepsilon_k \phi_k(\mathbf{r})$, where $\hat{t} \equiv -\frac{1}{2}\nabla^2$ is the one-body kinetic energy operator.

With the ensemble formalism defined, we are now ready to define the terms in eq. (11). Recent work [43, 44, 46] has sought to rigorously define exact energy functionals for excited state ensembles, giving,

$$T_s^{\mathbf{w}}[n] := \sum_k f_k^{\mathbf{w}} \int \frac{1}{2} |\nabla \phi_k|^2 d\mathbf{r}, \quad (13)$$

$$E_H^{\mathbf{w}}[n] := \sum_{\kappa \kappa'} w_{\max(\kappa, \kappa')} U[n_{s, \kappa \kappa'}], \quad (14)$$

$$E_x^{\mathbf{w}}[n] := - \sum_{kk'} f_{\max(k, k')}^{\mathbf{w}} U[\phi_k \phi_{k'}^*] \quad (15)$$

Here, we used $\int \phi^* \hat{t} \phi d\mathbf{r} = \int \frac{1}{2} |\nabla \phi|^2 d\mathbf{r}$; $U[\rho]$ as defined earlier in Eq. (2); introduced $n_{s, \kappa \kappa'}(\mathbf{r}) = \langle \kappa_s | \hat{n}(\mathbf{r}) | \kappa_s \rangle$ as the density of Kohn-Sham state, $|\kappa_s\rangle$; and introduced $n_{s, \kappa \neq \kappa'}(\mathbf{r}) = \langle \kappa_s | \hat{n}(\mathbf{r}) | \kappa'_s \rangle$ as the (potentially complex-valued) transition density between Kohn-Sham states $|\kappa_s\rangle$ and $|\kappa'_s\rangle$.

The remaining energy, $E_c^{\mathbf{w}} := E^{\mathbf{w}} - \int n v d\mathbf{r} - T_s^{\mathbf{w}} - E_H^{\mathbf{w}} - E_x^{\mathbf{w}}$, is the unknown correlation energy functional. It is convenient to partition,

$$E_c^{\mathbf{w}}[n] := E_c^{\mathbf{w}, \text{SD}}[n] + E_c^{\mathbf{w}, \text{DD}}[n]. \quad (16)$$

into state-driven (SD) and density-driven (DD) components, each with different physical origins. [44–46] The density-driven term is always zero in pure states like polarized and unpolarized HEGs.

It is sometimes useful to rewrite eqs (14) and (15) as,

$$E_{H/x}^{\mathbf{w}} = \int n_{2, H/x}^{\mathbf{w}}(\mathbf{r}, \mathbf{r}') \frac{d\mathbf{r} d\mathbf{r}'}{2|\mathbf{r} - \mathbf{r}'|} \quad (17)$$

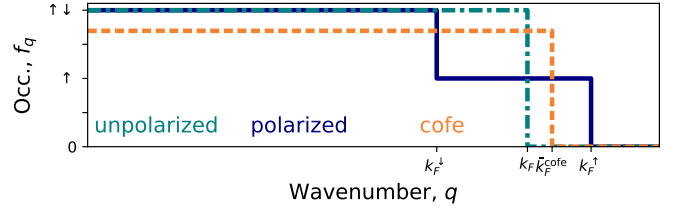


FIG. 1. Occupation factors as a function of wavenumber for an unpolarized gas (solid block), polarized gas ($\zeta = \frac{1}{2}$, solid line) and cofe gas (dotted line) – all at the same electron density.

using the ensemble Hartree and exchange pair-densities,

$$n_{2, H}^{\mathbf{w}}(\mathbf{r}, \mathbf{r}') = \sum_{\kappa \kappa'} w_{\max(\kappa, \kappa')} n_{s, \kappa \kappa'}(\mathbf{r}) n_{s, \kappa' \kappa}(\mathbf{r}'), \quad (18)$$

$$n_{2, x}^{\mathbf{w}}(\mathbf{r}, \mathbf{r}') = - \sum_{kk'} f_{\max(k, k')}^{\mathbf{w}} \rho_k(\mathbf{r}, \mathbf{r}') \rho_{k'}^*(\mathbf{r}, \mathbf{r}'), \quad (19)$$

where $\rho_k(\mathbf{r}, \mathbf{r}') = \phi_k(\mathbf{r}) \phi_k^*(\mathbf{r}')$. It is straightforward to see that using eqs (18) and (19) in (17) give the same energies as (14) and (15), respectively. Details and other helpful relationships for functionals will be introduced and used as required.

Before proceeding further, we make the important assumption that the results of Section II B apply to HEGs. This is an assumption because all EDFT results shown so far are for *finite* systems with *countable* numbers of excitations. By contrast, homogeneous electron gases are *infinite* and their excitations are *uncountable*. The rest of this manuscript treats HEGs as the appropriate thermodynamic limit of finite systems whose properties are consistent with the ensemble density functional theory presented in this section, and so obey straightforward generalizations of key equations.

III. CONSTANT OCCUPATION FACTOR HEGS

With core theory now established, let us proceed to explore generalizations of HEG physics that exploit the additional degrees of freedom from ensembles. Our aim is to develop an understanding of HEGs that spans ground- and excited-state physics. To that end, we will reveal the properties of “constant occupation factor ensemble” HEGs – the meaning of the name will soon become apparent. The key to generalizations is to invoke both ground and excited states of HEGs. As we shall show below, many properties are then uniquely determined by the occupation factors, f_q , of the HEG; while others depend on \mathbf{w} explicitly, so require some extra restrictions on the nature of excited states because there can be many different sets of weights, \mathbf{w} , that yield a given f_q .

Eqs (12), (13) and (15) reveal that the density, kinetic energy and exchange energy of any ensemble system depend explicitly only on the orbital occupation factors, $f_i^{\mathbf{w}}$. In HEGs, we replace $f_i^{\mathbf{w}}$ by f_q , i.e as a function

of absolute wavenumber, q . This follows from: i) the fact that the KS “orbitals” of an HEG are planewaves $\phi_{\mathbf{q}}(\mathbf{r}) \propto e^{i\mathbf{q}\cdot\mathbf{r}}$; and ii) that KS minimization dictates that we fill each $q = |\mathbf{q}|$ in full. Thus, given f_q it is possible to define the density, n , as well as the kinetic and exchange energies. We will therefore first discuss some HEGs from the perspective of orbital occupation factors; before proceeding to refine the definition.

The most intuitive form of HEG is an unpolarized gas in the lowest energy (ground) state. In orbital (KS) terms, the unpolarized HEG non-interacting ground state is a Slater determinant of doubly occupied plane-wave orbitals. Occupied states fill in \uparrow/\downarrow pairs up to a single Fermi wave number, k_F . Its wave-number dependent occupation factor and density are,

$$f_q^{\text{unpol}} = 2\Theta(k_F - q), \quad k_F = (3\pi^2 n)^{1/3}, \quad (20)$$

where $\Theta(x) = \{1 \forall x \geq 0; 0 \forall x < 0\}$ is a Heaviside step function. The density, n , of the gas is sufficient to describe the state.

Ground states realized by exposing the HEG to a uniform external magnetic field (the corresponding vector potential being ignored, as in spin-DFT) have a wave-number dependent occupation factor determined by spin-dependent Fermi wavenumbers,

$$f_q^{\text{pol}} = \Theta(k_F^{\uparrow} - q) + \Theta(k_F^{\downarrow} - q), \quad k_F^{\uparrow,\downarrow} = (6\pi^2 n_{\uparrow,\downarrow})^{1/3}. \quad (21)$$

The unpolarized gas is then the special case of $n_{\uparrow} = n_{\downarrow} = \frac{n}{2}$ giving $\zeta = 0$. A fully polarized gas has $n_{\uparrow} = n$, $n_{\downarrow} = 0$ and $\zeta = 1$. For definiteness, we work under the convention that the majority spin channel is the “up” (\uparrow) channel. The density, n , and spin-polarization, ζ , are sufficient to describe the state.

In this work, we consider (non-thermal) *ensembles* of excited states, which correspond to *averaged* occupation factors. Specifically, we consider ensembles obeying,

$$f_q^{\text{cofe}} = \bar{f}\Theta(\bar{k}_F^{\text{cofe}} - q), \quad \bar{k}_F^{\text{cofe}} = (6\pi^2 n/\bar{f})^{1/3} \quad (22)$$

The bar on top of \bar{f} (and, thus, \bar{k}_F) means that this quantity stems from an average w.r.t. an ensemble rather than to a pure state; and ‘cofe’ stands for ‘constant occupation factor ensemble’, [56] reflecting the fact that the system has the same occupation factor right up to a single (ensemble) Fermi level, unlike a polarized gas. We shall discuss below that the correct interpretation associates f_q^{cofe} with an *unpolarized* ensemble.

Before proceeding further, it is worth considering why we should choose f_q^{cofe} to be constant or zero, rather than any of the infinite number of other options we could have chosen. The main motivation is simplicity. Firstly, we aim to keep the number of parameters to two (n and \bar{f}) like the spin-polarized gas (n and ζ). We also aim to ensure that limiting cases (unpolarized and fully polarized gases) are reproduced by cofe gases – once adapted to inhomogeneous systems the limits respectively correspond to singlet ground states and ground and excited

states of one-electron systems. Finally, noting that both limits have the special feature that they yield constant occupation factors (two and one, respectively), we aim to retain this special feature in between the limits as a sensible generalization that incorporates excited states.

These three aims dictate the form of Eq. (22), as well as the kinetic and exchange energies of cofe HEGs. The addition of some extra restrictions (to be discussed below, as needed) on the excited states dictates the remaining properties of cofe-HEGs. As we shall see later in Section IV the resulting cofe gas is effective for predicting ground and excited states of inhomogeneous systems.

Figure 1 illustrates the different occupation factors for unpolarized, polarized and cofe HEGs, all at the same density n . The polarized gas has $\zeta = \frac{1}{2}$, while the cofe HEG has $\bar{f} = 1.7$. The unpolarized gas has a single Fermi level with double occupations, the polarized gas has two Fermi levels, one higher (\uparrow) and one lower (\downarrow) than that of the unpolarized gas, and is doubly occupied up to the lower level and then singly occupied to the higher level. The cofe gas also has a single Fermi level between the unpolarized and \downarrow levels, but is only partly occupied for all q . The choice of $\zeta = \frac{1}{2}$ and $\bar{f} = 1.7$ ensures that the polarized and cofe HEGs also have the same exchange energy – as can be seen by evaluating eqs (5) and (26).

Once we accept to deal with ensembles from constrained occupation factors, we can mix with equal weights a polarized HEG with its time-reversed partner. Nothing change in terms of the evaluation of the energy components. What changes is the interpretation. Now, we can find a continuum of *unpolarized* ensembles of cofe-HEGs, with energies that go from that of the regular unpolarized to that of the regular fully polarized HEGs. But the ensembles can also accommodate ground states *and* excited states (keeping in mind that the polarized gas is itself an excited state in the absence of a magnetic field), in a sense that will be clarified just below.

The ingredients of $\hat{\Gamma}^{\text{cofe}}$ are most easily understood by considering a finite system with four electrons:

- The unique unpolarized state is $|\text{unpol}\rangle = |1^2 2^2\rangle$, which is consistent with a Fermi level, $\bar{k}_F^{\text{cofe}} = \epsilon_2^+$, just above the second orbital energy. As a singular state we set $w_{\text{unpol}} = 1$ and obtain $f_1 = f_2 = \bar{f} = 2$.
- The fully polarized system, $|\text{fullpol}\rangle = |1^{\uparrow} 2^{\uparrow} 3^{\uparrow} 4^{\uparrow}\rangle$, is also unique ($w_{\text{fullpol}} = 1$). It has $\bar{k}_F^{\text{cofe}} = \epsilon_4^+$ (four orbitals allowed) and yields $f_1 = f_2 = f_3 = f_4 = \bar{f} = 1$. The corresponding state with all \downarrow -electrons has the same energetics (but time-reversed dynamics). Ensemble averaging the \uparrow - and \downarrow -spin systems therefore yields a net *unpolarized* system with the same energy terms.
- But, if we allow three orbitals, we have three maximally polarized ($N^{\uparrow} = 3$ and $N^{\downarrow} = 1$) states: $|\text{cofe}_0\rangle \equiv |1^2 2^{\uparrow} 3^{\uparrow}\rangle$, $|\text{cofe}_1\rangle \equiv |1^{\uparrow} 2^2 3^{\uparrow}\rangle$, and $|\text{cofe}_2\rangle \equiv |1^{\uparrow} 2^{\uparrow} 3^2\rangle$. Each state has a spin-polarization $\zeta_{\text{eff}} = \frac{3-1}{4} = \frac{1}{2}$. The (non-interacting) Fermi level, k_F^{\uparrow} ,

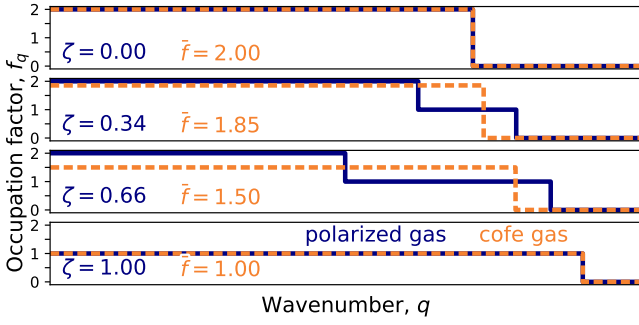


FIG. 2. Like Figure 1 except showing polarized and coFe HEGs at a variety of ζ and \bar{f} . Note that the polarized and coFe gas are, as expected, the same for $\zeta = 0$ and $\bar{f} = 2$, or $\zeta = 1$ and $\bar{f} = 1$.

for \uparrow electrons is always $k_F^\uparrow = \epsilon_3^+$. But, we cannot define a level for \downarrow electrons due to holes in $|\text{coFe}_1\rangle$ and $|\text{coFe}_2\rangle$. Assigning each of the three states an equal weight, $w_0 = w_1 = w_2 = \frac{1}{3}$, yields $f_1 = f_2 = f_3 = \frac{4}{3}$, as desired. Thus, $\bar{k}_F^{\text{coFe}} = k_F^\uparrow (= k_F^\downarrow) = \epsilon_3^+$ (after we also average over spin) for the whole ensemble.

Replacing orbital indices by \mathbf{q} , and taking the limit $N, V \rightarrow \infty$ for fixed density, $n = \frac{N}{V}$, and ensemble Fermi level, \bar{k}_F , yields the actual coF ensemble. It is composed of ground and excited states all with the same polarization, $\zeta_{\text{eff}} = 2/\bar{f} - 1$, (and their time reversed partners) where $\bar{f} = 6\pi^2 n \bar{k}_F^{-3}$ follows from eq. (22). Sections IIIB and IIID will expand a little on the specifics of states required for coFe HEGs. Here and henceforth we drop the superscript from \bar{k}_F^{coFe} , and simply use \bar{k}_F .

It is finally worth noting that the energy of a coFe HEG with $\bar{f} = 2$ is always equal to that of an *unpolarized* gas with $\zeta = 0$, while the energy of a coFe HEG with $\bar{f} = 1$ is always equal to that of a *fully polarized* gas with $\zeta = 1$ (keeping in mind that the ensemble averages over the time-reversed state). Figure 2 shows f_q for a selection of polarized and coFe gases between (and at) these limits, all yielding the same density, n . Values of ζ and \bar{f} are ‘paired’ to yield the same exchange energy – we will later exploit this pairing in eq. (42) of Section IIID.

We will next proceed to compute the energy components of the coFe HEG. Key results are summarized in Table I.

A. Density, kinetic and exchange energies

The density, $n[f_q] := \int_0^\infty f_q \frac{q^2 dq}{2\pi^2}$, and kinetic energy per particle,

$$t_s[f_q] := \frac{1}{n[f_q]} \int_0^\infty f_q \frac{q^2}{2} \frac{q^2 dq}{2\pi^2}. \quad (23)$$

of an HEG are direct functionals of the occupation factor distribution, f_q . Prefactors deal with normaliza-

tion of the orbitals and energies. The kinetic energy integral follows from the fact that $\phi_{\mathbf{q}}^*(\mathbf{r})[-\frac{1}{2}\nabla^2\phi_{\mathbf{q}}(\mathbf{r})] = \frac{1}{2}q^2\phi_{\mathbf{q}}^*(\mathbf{r})\phi_{\mathbf{q}}(\mathbf{r})$.

Typically we are interested in some fixed density, $n = \frac{3}{4\pi r_s^3}$, defined by its Wigner-Seitz radius, r_s , which imposes constraints on f_q (e.g. the Fermi levels in the previous section). Throughout we will implicitly define all HEGs to be at fixed Wigner-Seitz radius, r_s , and vary other parameters under this assumption. Using the occupation factor model for a polarized gas with fixed ζ and r_s yields the kinetic energy given by eq. (4).

Consider instead a coFe HEG, where f_q is given by eq. (22). We obtain, $n[f_q] = \frac{\bar{f}\bar{k}_F^3}{6\pi^2}$ from which we confirm that $\bar{k}_F = (6\pi^2 n/\bar{f})^{1/3}$. The kinetic energy of a coFe HEG therefore has the separable expression,

$$t_s^{\text{coFe}}(r_s, \bar{f}) = \frac{3\bar{k}_F(r_s, \bar{f})^2}{10} = t_s(r_s) \left[\frac{2}{\bar{f}} \right]^{2/3}, \quad (24)$$

using $t_s(r_s)$ from eq. (6).

In addition to the density and kinetic energy, the exchange energy of any HEG may also be evaluated directly from f_q . Replacing sums over k and k' by integrals over \mathbf{q} and \mathbf{q}' lets us rewrite Eq. (15) as,

$$\epsilon_x[f_q] := -\frac{1}{n[f_q]} \int_0^\infty \int_0^\infty f_{\max(\mathbf{q}, \mathbf{q}')} V(\mathbf{q}, \mathbf{q}') \frac{q'^2 dq'}{2\pi^2} \frac{q^2 dq}{2\pi^2}, \quad (25)$$

where, $V(\mathbf{q}, \mathbf{q}') = \int_{-1}^1 \frac{\pi dx}{q^2 + q'^2 - 2qq'x} = \frac{\pi}{qq'} \log \frac{|q+q'|}{|q-q'|}$ is the spherically averaged Coulomb potential. A little additional work on the integral (see Appendix A for details) yields eq. (5) for a polarized gas; and,

$$\epsilon_x^{\text{coFe}}(r_s, \bar{f}) = -\frac{\bar{f}}{n} \int_0^{\bar{k}_F} \frac{q}{\pi} \frac{q^2 dq}{2\pi^2} = \epsilon_x(r_s) \left[\frac{2}{\bar{f}} \right]^{1/3}, \quad (26)$$

for coFe HEGs, where $\epsilon_x(r_s)$ is the unpolarized HEG expression of eq. (7).

Although not necessary for computing, ϵ_x , we may similarly derive an expression for the HEG exchange hole, defined in eq. (19). We obtain,

$$n_{2,x}^{\text{coFe}}(R; r_s, \bar{f}) = \Pi_x^{\text{coFe}}(r_s, \bar{f}) N(\bar{k}_F R) \quad (27)$$

where,

$$\Pi_x^{\text{coFe}}(r_s, \bar{f}) = -\bar{f} \int_0^{\bar{k}_F} \frac{q^3}{3\pi^2} \frac{q^2 dq}{2\pi^2} = \frac{-n^2}{\bar{f}} \quad (28)$$

is the on-top pair-density of the exchange hole, and $N(x) := 9[\sin(x) - x \cos(x)]/x^6$ is a function. We will use the relationship between the exchange energy and exchange hole to help in deriving the properties of the Hartree energy, in the next section.

B. Hartree energy

The ensemble Hartree energy functional is given in eq. (14). This term is usually ignored in HEG discussions because $n_{2,H} = n^2$ in polarized and unpolarized gases at arbitrary ζ , which means that ϵ_H exactly cancels the energy of the positive background charge, ϵ_{bg} – that is, $\epsilon_H[n_{2,H} = n^2] = -\epsilon_{bg}$. In coFe HEGs this cancellation is incomplete. The singular background charge is guaranteed, by charge neutrality, to be cancelled in full. However, the Hartree pair-density, $n_{2,H}^w \neq n^2$, differs from the background charge density, n^2 , and thus ϵ_H^w includes additional terms. The energy per particle of an ensemble HEG is,

$$e^w[f_q^w] := t_s[f_q^w] + \Delta\epsilon_H^w[f_q^w] + \epsilon_x[f_q^w] + \epsilon_c^w[f_q^w], \quad (29)$$

where superscripts w indicate an explicit dependence on the nature of the ensemble. The additional positive Hartree energy contribution,

$$\Delta\epsilon_H^w = \epsilon_H^w - \epsilon_{bg} = \frac{1}{n} \int \Delta n_{2,H}^w(R) \frac{dR}{2R}, \quad (30)$$

may be evaluated [eqs (17) and (18)] using the ensemble Hartree pair-density deviation, $\Delta n_{2,H}^w = n_{2,H}^w - n^2$.

We therefore seek closed-form expressions for $n_{2,H}^{\text{coFe}}$ and $\Delta\epsilon_H^{\text{coFe}}$ for the special case of a coFe HEGs with maximal polarization within the ensemble, as defined earlier. Full details for Hartree expressions are rather involved so have been left to Appendix B. The rough argument is as follows: 1) the background charge is cancelled by $\kappa = \kappa'$ terms in (14) or (18), so we need only evaluate $\kappa \neq \kappa'$ terms; 2) the coFe ensemble states, $|\kappa\rangle$, contain every possible combination of paired and unpaired orbitals up to \bar{k}_F ; 3) each of these states is weighted equally; 4) we may therefore use combinatorial arguments to evaluate key expressions. The final step recognises that each state may be defined by a set, $\{\mathbf{q}\}_{\text{double}}$, of doubly occupied orbitals, such that the remaining occupied orbitals (with $|\mathbf{q}| \leq \bar{k}_F$) contain only an \uparrow electron. Each non-interacting state is then a Slater determinant consistent with the occupations, whose properties may be understood via $\{\mathbf{q}\}_{\text{double}}$ and \bar{k}_F .

Appendix B yields, $\Delta\epsilon_H^{\text{coFe}}(r_s, \bar{f}) := \frac{C_H}{r_s} \frac{(2-\bar{f})(\bar{f}-1)}{\bar{f}^{4/3}}$, [eq. (B8)] where $C_H = 2^{1/3}C_x$. We rewrite this as,

$$\Delta\epsilon_H^{\text{coFe}}(r_s, \bar{f}) = |\epsilon_x(r_s, \bar{f})| \frac{(2-\bar{f})(\bar{f}-1)}{\bar{f}}, \quad (31)$$

for use in eq. (29) and later expressions. This result follows from the fact that,

$$n_{2,H}^{\text{coFe}}(R; r_s, \bar{f}) = n^2 + \Delta\Pi_H^{\text{coFe}}(r_s, \bar{f})N(\bar{k}_F R), \quad (32)$$

$$\Delta\Pi_H^{\text{coFe}}(r_s, \bar{f}) = n^2 \frac{(2-\bar{f})(\bar{f}-1)}{\bar{f}^2} = -\frac{(2-\bar{f})(\bar{f}-1)}{\bar{f}} \Pi_x^{\text{coFe}}, \quad (33)$$

where $N(x)$ is the same expression used in (27).

C. Energies in the low-density limit

We cannot analytically evaluate the energy of an HEG at arbitrary density, n . We can, however, semi-analytically evaluate it in the high density (large n , small r_s) and low density (small n , large r_s) limits. The high density limit may be obtained from a series solution around the Kohn-Sham solution. In the low density limit, the electrons are far enough apart to undergo a process known as a Wigner crystallisation. [57, 58] The resulting “strictly correlated electron” physics may then be understood via a classical leading order term, with quantum corrections. The transition occurs at $r_s \approx 100$ Bohr.

Recent work [47] has shown that any dependence on ensemble properties must vanish in the low-density limit of any finite system; so that *all excited state properties become degenerate to both leading and sub-leading order*. It is very likely that this result also holds true in the thermodynamic limit of HEGs, as justified by the following intuition:

1. As the density becomes small, the distance between electrons becomes large and the particles become effectively classical with a quantum state defined by fluctuations around a classical minima;
2. Whether the system is finite, or infinite, the fluctuations may be “excited” any number of times with no impact on the *classical* leading order term of the interaction energy;
3. Furthermore, the next leading order *quantum* correction from zero-point energy fluctuations around the classical minima are dictated only by the density constraint, and are therefore also independent of excitation structure.

This result has important implications for both spin-polarized and coFe HEGs, as both may be represented as ensemble of excited states – with specific properties governed by ζ or \bar{f} , respectively. It follows from the above that the leading two orders of their low-density energies are independent of the excitation structure. Consequently, energies are independent of \bar{f} and ζ . Independence of ζ has long been theorized for spin-polarized HEGs. Recent QMC data [59] provides confirmation of this result.

The leading order terms correspond to $1/r_s$ and $1/r_s^{3/2}$ in the usual large- r_s series description of HEGs. Therefore, ensemble and spin effects can only contribute at $O(1/r_s^2)$. The (Hartree) exchange- and correlation energy of strictly correlated electrons in the low-density limit (ld) therefore obeys $\lim_{r_s \rightarrow \infty} \epsilon_{Hxc}(r_s, \zeta) = \epsilon_{Hxc}^{\text{ld}}(r_s)$, where,

$$\epsilon_{Hxc}^{\text{ld}}(r_s) := \frac{-C_\infty}{r_s} + \frac{C'_\infty}{r_s^{3/2}} + \dots, \quad (34)$$

includes only the part of the Hartree energy that is not cancelled by background charge. The best esti-

mates for coefficients are $C_\infty = 0.8959 \approx 1.95C_x$ and $C'_\infty = 1.328$. [60, 61]

In regular HEGs, the Hartree term is fully cancelled by background charge so can be ignored. For polarized HEGs we therefore obtain, $\lim_{r_s \rightarrow \infty} \epsilon_c = \epsilon_{\text{Hxc}}^{\text{ld}} - \epsilon_x$, and,

$$\lim_{r_s \rightarrow \infty} \epsilon_c(r_s, \zeta) := \frac{-C_\infty + C_x f_x(\zeta)}{r_s} + \frac{C'_\infty}{r_s^{3/2}} + \dots, \quad (35)$$

using f_x from eq. (5). By contrast, in a cofe HEG there is a non-zero component ($\Delta\epsilon_{\text{H}}^{\text{cofe}}$) in the Hartree energy. It therefore follows that, $\lim_{r_s \rightarrow \infty} \epsilon_c^{\text{cofe}} = \epsilon_{\text{xc}}^{\text{ld}} - \Delta\epsilon_{\text{H}}^{\text{cofe}} - \epsilon_x^{\text{cofe}}$. We finally obtain,

$$\lim_{r_s \rightarrow \infty} \epsilon_c^{\text{cofe}}(r_s, \bar{f}) = \frac{-C_\infty + C_x f_{\text{Hx}}^{\text{cofe}}(\bar{f})}{r_s} + \frac{C'_\infty}{r_s^{3/2}} + \dots, \quad (36)$$

where,

$$f_{\text{Hx}}^{\text{cofe}}(\bar{f}) = \left[\frac{2}{\bar{f}} \right]^{1/3} \frac{(\bar{f} - 1)^2 + 1}{\bar{f}}, \quad (37)$$

follows from eqs (26) and (31). This is the appropriate low-density series expansion for the correlation energy of cofe HEGs.

D. State-driven correlation energies

In general, the correlation energy of an ensemble is separable into two terms, [44, 45]

$$E_c^{\mathbf{w}} := E_c^{\mathbf{w}, \text{SD}} + E_c^{\mathbf{w}, \text{DD}}, \quad (38)$$

where each covers different physics of the ensemble. The “state-driven” (SD) term is the *only term present* in pure states, such as polarized gases. In general ensembles, it is like a weighted average of conventional correlation energies for the different states of the ensemble. The “density-driven” (DD) term reflects the fact that the densities of the individual Kohn-Sham and interacting states that form the ensemble are not necessarily the same – only the averaged ensemble density is the same.

We expect that only the SD part of the correlation energy should form part of the xc energy used in density functional approximations, so focus here on this term – we explain this choice in Section IV. Our goal is therefore to determine $\epsilon_c^{\text{SD,cofe}}(r_s, \bar{f})$ as a function of r_s and \bar{f} , which we will use as a basis for parameterization in the next section. This involves considering the high- and low-density limits of matter (and therefore cofe-HEGs), for which exact results will be derived. We will also discuss how to repurpose existing data for values in between these limits. Comprehensive analysis of both state- and density-driven correlation terms is reported in Appendix C. Below, we summarize key elements of the SD correlation energy analysis.

The division into SD and DD terms is not unique, [44–46] and any explicit study of the separation into SD and DD terms requires accessing the properties of a variety of excited states of *interacting* HEGs. Nevertheless, discussion near eq. (14) of Ref. 46 argues that the SD correlation energy may be written in adiabatic connection and fluctuation-dissipation theorem (ACFD) form:

$$\epsilon_c^{\text{SD}} := \frac{1}{n} \int_0^1 d\lambda \int_0^\infty \frac{-d\omega}{\pi} \int \frac{d\mathbf{r} d\mathbf{r}'}{2|\mathbf{r} - \mathbf{r}'|} \times [\chi_\lambda(\mathbf{r}, \mathbf{r}'; i\omega) - \chi_0(\mathbf{r}, \mathbf{r}'; i\omega)]. \quad (39)$$

Here, χ_0 is the collective density-density response of the non-interacting cofe HEG defined earlier – i.e. the ensemble of part-polarized ground- and excited states that yield \bar{f} . χ_λ is its equivalent to a scaled Coulomb interaction $\frac{1}{R} \rightarrow \frac{\lambda}{R}$. In principal, the individual states in the interacting ensemble may be followed from their known $\lambda = 0$ values to their unknown value at arbitrary λ , although this is not required in practice.

The key step toward understanding how to separate and parametrise terms is to use the random-phase approximation (RPA). RPA becomes exact (to leading order) in the high-density limit. [10] More generally, RPA provides an approximate solution for eq. (39), and thus provides insights into the SD correlation term. Details are provided in Appendix C 1. Key findings are: i) that, $\epsilon_c^{\text{SD,cofe}}$ is approximately linear in \bar{f} for high densities; ii) for low densities we obtain a scaling that is similar to $f_x^{\text{cofe}}(\bar{f})$. Appendix C 2 then uses the RPA results, and fundamental theory, to argue that,

$$\epsilon_c^{\text{SD,cofe,hd}}(r_s, \bar{f}) = (\bar{f} - 1)\epsilon_c(r_s, 0) + (2 - \bar{f})\epsilon_c(r_s, 1), \quad (40)$$

$$\epsilon_c^{\text{SD,cofe,ld}}(r_s, \bar{f}) = \epsilon_x(r_s) \left[\frac{C_\infty}{C_x} - f_x^{\text{cofe}}(\bar{f}) \right] + \frac{C'_\infty}{r_s^{3/2}}, \quad (41)$$

are, respectively, the exact high- and low-density limits of ϵ_c^{cofe} . That is, $\lim_{r_s \rightarrow 0} \epsilon_c^{\text{SD,cofe}}(r_s, \bar{f}) = \epsilon_c^{\text{SD,cofe,hd}}(r_s, \bar{f})$ and $\lim_{r_s \rightarrow \infty} \epsilon_c^{\text{SD,cofe}}(r_s, \bar{f}) = \epsilon_c^{\text{SD,cofe,ld}}(r_s, \bar{f})$.

Filling in the gaps between these limits requires quantum Monte Carlo (QMC) calculations: which, however, are *only available for spin-polarized ground-states* of homogenous gases. Appendix C 2 therefore shows how to reuse existing spin-polarized QMC data for the in-between regime, by adapting it for cofe HEGs. Specifically, it argues that,

$$\epsilon_c^{\text{SD,cofe,mhd}}(r_s, \bar{f}) \equiv \epsilon_c^{\text{QMC}}(r_s, \zeta = \hat{f}_{\text{x-map}}^{-1}(\bar{f})) \quad (42)$$

is a reasonable *approximation* for medium-high densities (mhd). The key assumption behind this relationship is that HEGs with same exchange energy should have a similar state-driven correlation energy. Thus, $\hat{f}_{\text{x-map}}(\zeta)$ is a function yielding, $\epsilon_x^{\text{cofe}}(r_s, \hat{f}_{\text{x-map}}(\zeta)) = \epsilon_x(r_s, \zeta)$ and $\epsilon_x^{\text{cofe}}(r_s, \bar{f}) = \epsilon_x(r_s, \hat{f}_{\text{x-map}}^{-1}(\bar{f}))$. Eq. (42) becomes exact in the low-density limit, but incorrect in the high-density limit. More information is provided in Appendix C 2.

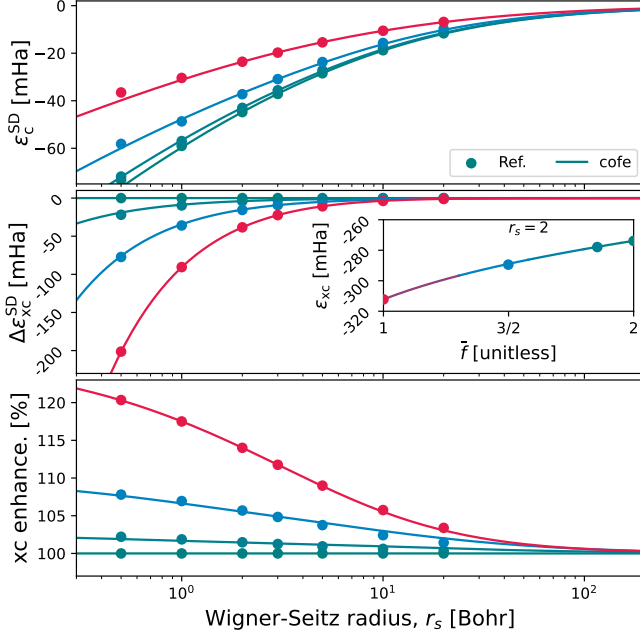


FIG. 3. Correlation (top) and xc (middle) energies and xc (bottom) enhancement factors for HEGs as a function of r_s and $\bar{f} \in (2, 1.85, 1.50, 1)$. Plots show the cofe (solid lines) parametrization introduced here, and the adapted benchmark results from Ref. 8 (circles). The inset plot shows ϵ_{xc} (cofe and benchmark) as a function of \bar{f} , for $r_s = 2$. Line colours indicate the value of \bar{f} (see inset for values).

Appendix D details parametrization of $\epsilon_c^{\text{SD,cofe}}(r_s, \bar{f})$ for arbitrary densities, based on the theoretical work in this section. As an intermediate step, it also introduces approximations for $\hat{f}_{x\text{-map}}$ and its inverse, for use in eq. (42). Key results are visually summarized in Figure 3, which compares the parametrization of $\epsilon_c^{\text{SD,cofe}}$ with the (adapted) reference data used to fit it. The top plot shows correlation energies, $\epsilon_c^{\text{SD,cofe}}(r_s, \bar{f})$. The middle plot shows deviations, $\Delta\epsilon_{xc}^{\text{SD,cofe}} = \epsilon_{xc}^{\text{SD,cofe}}(r_s, \bar{f}) - \epsilon_{xc}^{\text{SD,cofe}}(r_s, 2)$, from unpolarized gas values. The bottom plot shows xc enhancement factors, $\epsilon_{xc}^{\text{SD,cofe}}(r_s, \bar{f})/\epsilon_{xc}^{\text{SD,cofe}}(r_s, 2)$, which must approach one (100%) in the low-density (large r_s) limit.

IV. FROM COFE-HEG TO REAL, INHOMOGENEOUS SYSTEMS

A. Adaptation to inhomogeneous systems

The main application of HEG work is as the foundation for approximations to inhomogeneous systems. Direct approximations based on Thomas-Fermi theory is generally not very effective for this purpose. But Kohn-Sham density functional approximations (DFAs) based on HEGs are wildly successful. What explains the difference? Kohn and Sham proposed to use an inhomogeneous

description of the (quantum mechanical) kinetic and (classical) Hartree energies, together with an HEG-based approximation for the exchange and correlation energies – see Eq. (1) and related discussion. It is natural to assume that ensembles will similarly benefit from a Kohn-Sham treatment, with the goal to extend the success of KS-based approximations for ground states to excited states. Therefore, we write

$$E_{\text{eLDA}}^w = \min_n \left\{ T_s^w[n] + \int n(\mathbf{r})v(\mathbf{r})d\mathbf{r} + E_H^w[n] + \int n(\mathbf{r})\epsilon_{xc}^{\text{cofe}}(r_s(\mathbf{r}), \bar{f}(\mathbf{r}))d\mathbf{r} \right\}. \quad (43)$$

Here, we have replaced pure state T_s and E_H by their ensemble equivalents, T_s^w [eq. (13)] and E_H^w [eq. (14)]; and locally approximated the xc energy by the cofe LDA with local Wigner-Seitz radius, $r_s(\mathbf{r})$, and local effective occupation factor, $\bar{f}(\mathbf{r})$ – to be discussed below.

In practical terms, it is usually better to use a state-specific DFA, rather than an ensemble. Eq. (43) may be adapted to a state-specific form [41] by defining $E_{\kappa}^{\text{eLDA}} := \partial_{w_{\kappa}} E_{\text{eLDA}}^w$ (for any positive weight, w_{κ} , in the ensemble). Then, target state $|\kappa\rangle$ has energy,

$$E_{\kappa}^{\text{eLDA}} = T_s[n_{\kappa}] + \int n_{\kappa}(\mathbf{r})v(\mathbf{r})d\mathbf{r} + E_{H,\kappa}[n_{\kappa}] + \int n_{\kappa}(\mathbf{r})\epsilon_{xc}^{\text{cofe}}(r_{s,\kappa}(\mathbf{r}), \bar{f}_{\kappa}(\mathbf{r}))d\mathbf{r}, \quad (44)$$

where $E_{H,\kappa} := \partial_{w_{\kappa}} E_H^w$ is its ensemble Hartree energy; and we evaluate the energy using the Wigner-Seitz radius and effective occupation factor from n_{κ} .

The above approximation ignores density-driven (DD) correlations entirely. i.e. sets $E_c^w, \text{DD} \equiv 0$, with the assumption that they are small. More fundamentally, this choice comes from the fact that the use of exact Hartree [Eq. (14); defined by the fluctuation dissipation theorem] is equivalent to a physical argument that HEGs should only be used to approximate response-like properties of systems [46] – consistent with work on ground state KS-DFT. Density-driven correlations are Hartree-like [44–46] so, by the same argument, should *also* be treated via the inhomogeneous system — not from an HEG. Therefore,

$$\epsilon_{xc}^{\text{cofe}}(r_s, \bar{f}) := \epsilon_x^{\text{cofe}}(r_s, \bar{f}) + \epsilon_c^{\text{SD,cofe}}(r_s, \bar{f}), \quad (45)$$

involves only the state-driven correlation energy. From Appendix D, we see that the exchange energy term takes the exact form,

$$\epsilon_x^{\text{cofe}}(r_s, \bar{f}) := \epsilon_x(r_s)[2/\bar{f}]^{1/3} \quad (46)$$

while the state-driven correlation energy term may be parametrized as,

$$\epsilon_c^{\text{SD,cofe}}(r_s, \bar{f}) := (\bar{f} - 1)\epsilon_c^0 + (2 - \bar{f})\epsilon_c^1 + (\bar{f} - 1)(2 - \bar{f})[M_2(r_s) + (\frac{3}{2} - \bar{f})M_3(r_s)] \quad (47)$$

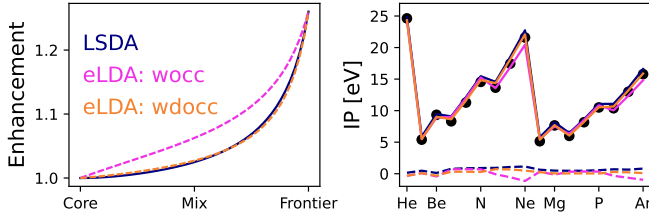


FIG. 4. Left: Enhancement factor for different ratios of core and frontier occupied orbitals from LSDA (teal); and eLDA with effective \bar{f} from Eq. (48) (wocc, magenta) and Eq. (49) (wdocc, orange). Right: Ionisation potentials (IPs) for atoms He–Ar using a conventional LSDA [9] (navy), Eq. (48) (magenta) and Eq. (49) (orange). Dashed lines indicate deviations from experimental IPs.

for ϵ_ζ^ζ computed using eq. (D4) (parameters in Table II). Here, $M_{2,3}(r_s)$ involve weighted sums (coefficients in Table III) over functions, ϵ_ζ^ζ .

All expressions except $\bar{f}(\mathbf{r})$ are thus known. The *final step* demands that we make an ansatz for $\bar{f}(\mathbf{r})$ that correctly reproduces the properties of a coFe-HEG, but is also effective for many-electron systems. A natural first guess is to employ a density-weighted average of occupation factors,

$$\bar{f}^{\text{wocc}}(\mathbf{r}) := \sum_i f_i^w \frac{f_i^w n_i(\mathbf{r})}{n(\mathbf{r})} = \frac{\sum_i (f_i^w)^2 n_i(\mathbf{r})}{\sum_i f_i^w n_i(\mathbf{r})}. \quad (48)$$

Here, $n_i = |\phi_i|^2$ is the density of orbital ϕ_i , and f_i^w is its occupation factor in the ensemble. It is easily verified that this ansatz is exact for any coFe HEG, so is *prima facie* a reasonable extension to inhomogeneous systems.

However, testing (to be discussed below) reveals that this ansatz can yield poor results for ground states. These errors come from the effective spin-enhancement being too great in regions that are partly-polarized [i.e. where $1 < \bar{f}(\mathbf{r}) < 2$]. Fortunately, we may exploit the fact that there are other choices of inhomogeneous $\bar{f}(\mathbf{r})$ that yield correct behaviour in HEGs, but that do not hamper performance in inhomogeneous ground states.

We therefore (see Supp. Mat. Sec. I [62] for details) instead adopt a double weighted average,

$$\bar{f}^{\text{dwocc}}(\mathbf{r}) := \frac{\sum_i (f_i^w)^{1/3} n_i(\mathbf{r})}{\sum_i f_i^w n_i(\mathbf{r})} \frac{\sum_i (f_i^w)^{8/3} n_i(\mathbf{r})}{\sum_i f_i^w n_i(\mathbf{r})}, \quad (49)$$

for calculations. The form is chosen to closely match the spin-enhancement of exchange in doublets and thus extend the perfect (by construction) replication of LSDA in one-electron (doublet) systems by an approximate replication of LSDA in general doublet systems.

The left panel of Figure 4 illustrates the importance of choosing \bar{f} appropriately. It shows the exchange enhancement factor of a doublet system (density $n = 2n_{\text{Core}} + n_{\text{Frontier}}$), for different ratios of $n_{\text{Frontier}}/n_{\text{Core}}$, using standard spin-polarization, and ensemble enhancement with Eqs (48) and (49). It is clear that (48) over-

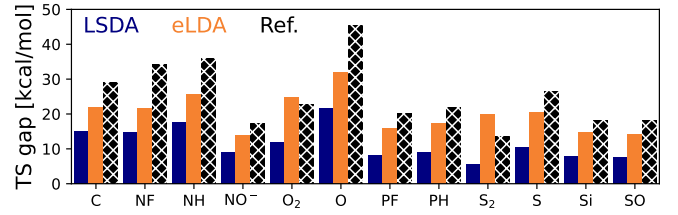


FIG. 5. Triplet–singlet gaps in atoms and diatomic systems from LSDA (navy) and eLDA (orange) calculations, compared to experimental reference data (black with crosses). LSDA and reference data from Ref. 67. TDLDA gaps are too large for the figure, so have been left out.

enhances exchange in general, relative to LSDA. By contrast, (49) matches quite closely to the spin-polarized enhancement of LSDA for all ratios.

How well does eLDA work in practice? The next sections will address excited state energies. *But, first, we need to ensure that the eLDA does not make things worse for ground state energies.* The right panel of Figure 4 therefore shows the ionization potentials (IPs) of atoms – that is the difference in ground state energies between the atom and its cation – computed with Eq. (43) using Eq. (48) and Eq. (49). IPs provide a useful test of $\bar{f}(\mathbf{r})$ on ground states because the occupation factors of atoms and ions are always different and at least one system always involves an unpaired electron.

The figure reveals that Eq. (49) yields results that are consistently close to standard LSDA calculations, whereas (48) leads to much greater deviations in some cases. We therefore see that using (49) yields good (relative to LSDA) performance on ground states; and use Eq. (49) for our inhomogeneous effective occupation factor in all subsequent calculations.

Technical details for all atomic and molecular calculations for ground and excited states are in Supp. Mat. Sec. II [62]. For now it suffices to say that we carry out LSDA and time-dependent LDA (TDLDA) calculations using standard self-consistent field (SCF) approaches implemented in `psi4` [63, 64] and `pyscf`, [65, 66] but evaluate eLDA calculations using an orbital optimized approach with `psi4` as an ‘engine’. Spin and spatial symmetries are preserved in eLDA calculations, except for atoms which are evaluated using cylindrical spatial symmetries for consistency with standard quantum chemistry codes and practice.

B. Low-lying excitations in molecules

With the eLDA established and validated on ground state systems, we are ready to test its predictive ability for excitations. As a first test, (Figure 5) we consider the twelve triplet-singlet gaps in biradicals of the TS12 [68] dataset. The performance of PW92 [10] energy differences (referred to as ΔSCF calculations, to differentiate

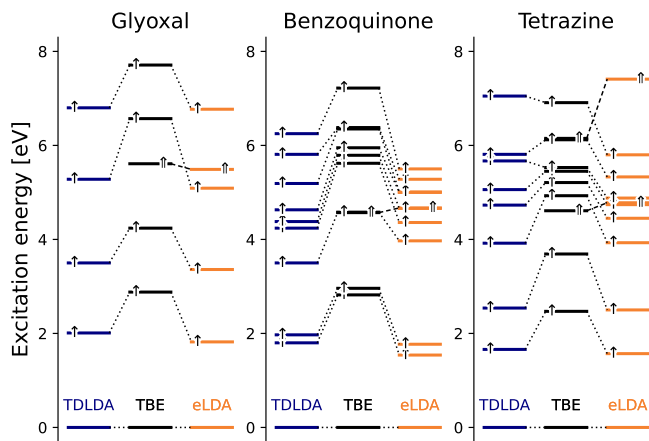


FIG. 6. Low-lying spectra (singlets only) of glyoxal, benzoquinone and tetrazine predicted using TDLDA (navy) and eLDA (orange); compared against theoretical best estimate (TBE) values. [69] Connections between spectrum in approximations and TBE are shown using dotted lines, to facilitate comparisons. TDLDA captures single excitations (indicated by single arrows on the level line) but misses the double excitations (double arrows) entirely so these connections are excluded from the plot.

from TDLDA calculations) on this dataset was explored in Ref. 67, using restricted, unrestricted and complex orbital Kohn-Sham theory. The mean-signed errors (root mean squared errors) from Δ SCF calculations are -13.7 (14.5) kcal/mol using LSDA (i.e. unrestricted Kohn-Sham theory); and 10.9 (11.5) kcal/mol for restricted theory. Employing complex orbitals reduces these LDA errors substantially, to -1.2 (2.2) kcal/mol, albeit at the expense of non-idempotent density matrices.

Using the eLDA formalism developed here (also a Δ SCF method) to compute the gaps yields errors of -5.0 (7.4) kcal/mol – respectable statistics and a major improvement on LSDA, as shown in Figure 5. Indeed, eLDA is closer in quality to the complex orbital performance than LDA or LSDA performance, despite eLDA being a ‘restricted’ theory that preserves idempotency (unlike complex orbitals) and avoids spin-contamination issues (unlike unrestricted KS).

By contrast, evaluating TDLDA (using VWN correlation [9] for consistency with other results) on the triplet ground states yields enormous errors of 77.2 (88.6) kcal/mol – with the predicted gaps being too large to include in the figure. eLDA thus out-performs both ground state (LSDA) and excited state (TDLDA) LDA-based calculations, despite being constrained to yield desirable physical properties of the true KS solution.

Continuing on the theme of predicting difficult excitations, let us consider some excitations that TDLDA cannot predict at all: double excitations. Double excitations are singlet excited states in which the interacting wave function is dominated by a Slater determinant with paired orbitals, and in which one pair is ‘doubly promoted’ from the dominant ground state Slater determi-

nant (e.g. $|\phi_0^2\phi_1^2\phi_3^2\rangle$ instead of $|\phi_0^2\phi_1^2\phi_2^2\rangle$ for a six-electron system). They are *impossible* to predict using the adiabatic approximation that is employed in all practical implementations of time-dependent DFT. [20, 21]

Figure 6 shows the low-lying singlet spectra of some selected molecules, computed using adiabatic time-dependent LDA (TDLDA) and eLDA. We choose glyoxal, benzoquinone and tetrazine from the QuestDB dataset, [69] as their low-lying spectra includes difficult-to-predict double excitations for which high-quality theoretical best estimates (TBE) results are available. They therefore serve as good examples to compare the eLDA approach with its TDLDA counterpart.

It is immediately clear that, for the lowest-lying excitations involving single promotion of an electron (“single excitations”, single arrows), eLDA predicts similar excitation energies to TDLDA and thus has similar performance – albeit with a slight tendency to underestimate relative to TDLDA. However, unlike TDLDA, eLDA is also able to predict excitations involving *double* promotion of electrons (“double excitations”, double arrows) with a performance similar to that of single excitations. Thus, eLDA is nearly as good as TDLDA for low-lying excitations involving single promotion of an electron, but is also able to predict double promotions, unlike TDLDA. It therefore offers a major advance on TDLDA.

Figure 6 also provides evidence that eLDA can be a cornerstone theory for better excited state approximations, based on the following argument. As can be seen from the figure, TDLDA and eLDA yield very similar energies for most single excitations. The similarity of TDLDA and eLDA energies suggests that *all regular DFAs* are likely to yield similar energies for these excitations, whether evaluated as TDDFAs or eDFAs – a theoretical justification for this argument is provided in Supp. Mat. Sec. III [62]. Thus, the thirty years of refinement of generalized gradient approximations (GGAs) and meta-GGAs (MGGAs) that has improved the quality of spectra predicted using TD(M)GGAs is likely to similarly improve spectra evaluated using e(M)GGAs. But e(M)GGAs may *also* exploit the extra degree of freedom enabled by the use of coe-gas physics and effective $\bar{f}(\mathbf{r})$.

In summary, we see that TDLDA fails quite dramatically for TS12 (Figure 5 and related discussion) and cannot capture double excitations (Figure. 6); in contrast to an excellent (TS12) or impressive (double excitations) performance from eLDA on the difficult excitations. Errors in single excitation spectra (Figure. 6) from TDLDA and eLDA are similar. Directly, this shows that eLDA either improves excited state predictions, or does not make them worse. Indirectly, it has positive implications for refinements to eLDAs, e.g. eGGAs or eMGGAs.

V. FUTURE PROSPECTS AND CONCLUSIONS

Ensemble density functional theory has recently benefited from a surge of fundamental understanding. This

has led to rapid advancements in extending, to excited states, the power of density functional theory for computing electronic structure of ground states. Especially, EDFT deals seamlessly with highly “quantum” states [41] (e.g. superpositions of Slater determinants and double excitations) of relevance to solar energy applications and quantum technologies.

However, despite an accumulation of successful applications, EDFT currently lacks a fully consistent framework for improving approximations: in the sense that it borrows density functional approximations (DFAs) which were originally designed for ground states as the key building blocks of the extended DFAs for excited states.

This work takes the first step toward *deriving a novel family of DFAs specifically designed for excitations*. It presents the cornerstone theory: the ‘cofe’ homogeneous electron gas (HEG) and the LDA for EDFT (eLDA). The ‘cofe’ HEG is developed using an unnoticed – thus, so far, unexplored – class of non-thermal ensemble states of the HEG. Analytic expressions of the relevant (defined by two parameters, like LSDA) energy components are reported in Table I. Some of these components have no analogues in regular DFT but find home and use in EDFT. High- and low-density limits of the correlation energy have been found analytically.

The eLDA is derived by dividing the DFT energy expression into terms that need to be treated using the inhomogeneous system, and those that are locally approximated using a cofe gas. Parametrisations for all terms required by the eLDA are derived and provided. An expression is also derived for the effective occupation factor of inhomogeneous systems, and is ‘normed’ on doublet systems.

The novel eLDA is then tested on a suite of important examples including ionization potentials, small triplet-singlet gaps, and low-lying excitations. These examples reveal that eLDA performs similarly to LSDA and/or time-dependent LDA (TDLDA) on problems where standard theories are known to work. However, it *also performs very effectively on problems where LSDA/TDLDA fail* – yielding excellent triplet-singlet gaps and impressive double excitation energies.

eLDA therefore readily offers an effective alternative to standard polarized-gas based theories for both ground and excited state problems. But, we stress that its true potential lies as the cornerstone for *better* models and methodologies. *What are the next natural steps to be considered?* We finish with three suggestions.

(1) It is vital to develop a generalized gradient approximation (GGA) for cofe-HEGs, to yield an eGGA along the lines of Eq. (43). The development of accurate GGAs in the late-1980s/early-90s greatly accelerated interest in DFT for ground states, by giving answers that were usefully predictive. eGGAs should do the same for excited states. Importantly, eGGAs would seamlessly integrate with existing hybrid-EDFT successes [40–42] and remove reliance on combination laws that (despite working unexpectedly well) are known to be incorrect for correla-

tion. [41] From there, additional steps may readily be taken up an *excited state* Jacob’s ladder, [15] to gain systematic improvements in excited state DFT modelling.

(2) The optimal way to model $\tilde{f}(\mathbf{r})$ remains an open problem, and is entangled with (1). It would be useful to understand why Eq. (49) works so much better than Eq. (48). Exploiting exact relationships, like combination laws, [41] is likely to lead to improved understanding and adaptation of $\tilde{f}(\mathbf{r})$ in inhomogeneous systems; and thus improvements to the predictive ability of eLDA and any eDFAs built on it.

(3) The cofe-gas is not the only excited state (ensemble) HEG that we could have used. As discussed in Section III it is a logical and simple *two*-parameter model that yields appropriate limits yet incorporates excited state physics. But, allowing for more parameters provides a wide scope for further generalizations. For example, one might separate the density into core (density, n_{core}) orbitals that are all double occupied, and use a cofe-like treatment for the remaining orbitals – yielding a three-parameter HEG governed by n , n_{core}/n and f that includes excited states.

Python code for studying and implementing the theory work in this manuscript is provided on Github <https://github.com/gambort/cofHEG>. Code to reproduce the atomic and molecular tests is available on request.

ACKNOWLEDGMENTS

TG was supported by an Australian Research Council (ARC) Discovery Project (DP200100033) and Future Fellowship (FT210100663). Computing resources were provided by the National Computing Merit Application Scheme (NCMAS sp13). TG and SP would like to thank Paola Gori-Giorgi for interesting discussions regarding homogeneous electron gases and their low density limit; useful discussions with Marco Govoni on a previous version of the manuscript are also acknowledged.

Appendix A: Exchange properties

Both ϵ_x and Π_x involve integrals of form,

$$\begin{aligned} X_2[f] &:= \int_0^\infty \int_0^\infty f_{\max(q,q')} A(q, q') \frac{q'^2 dq'}{2\pi^2} \frac{q^2 dq}{2\pi^2} \\ &= 2 \int_0^\infty \int_{q'}^\infty f_q A(q, q') \frac{q^2 dq}{2\pi^2} \frac{q'^2 dq'}{2\pi^2} \\ &= 2 \int_0^\infty \int_0^\infty \Theta(q - q') f_q A(q, q') \frac{q'^2 dq'}{2\pi^2} \frac{q^2 dq}{2\pi^2} \\ &= \int_0^\infty f_q \bar{A}(q) \frac{q^2 dq}{2\pi^2} \end{aligned} \quad (\text{A1})$$

where $A(q, q') = A(q', q)$ and,

$$\bar{A}(q) = 2 \int_0^q A(q, q') \frac{q'^2 dq'}{2\pi^2}$$

For ϵ_x we have $A(q, q') = V(q, q')$ where $\bar{V}(q) = 2 \int_0^q V(q, q') \frac{q'^2 dq'}{2\pi^2} = \frac{q}{\pi} \int_0^1 \log \frac{|1+x|}{|1-x|} x dx = \frac{q}{\pi}$. We thus obtain eq. (25) of the main text. To compute Π_x we can set $A(q, q') = 1$ where $\bar{1}(q) = 2 \int_0^q \frac{q'^2 dq'}{2\pi^2} = \frac{q^3}{3\pi^2}$ and so we can easily compute Π_x given f_q . For coe HEGs we obtain eqs (26) and (28).

The case of $n_{2,x}(R)$ is also covered by (A1), by setting $A(q, q'; R) = \int e^{i(\mathbf{q}-\mathbf{q}') \cdot \mathbf{R}} \frac{d\mathbf{q}}{4\pi} \frac{d\mathbf{q}'}{4\pi}$. However, this is rather painful to deal with in general. The special case of coe HEGs is more easily handled by recognising that $f_{\max(q, q')} = \bar{f} \Theta(k_F - q) \Theta(k_F - q')$. Then,

$$n_{2,x}^{\text{cofe}}(R) = -\bar{f} \int_0^{\bar{k}_F} e^{i\mathbf{q} \cdot \mathbf{R}} \frac{d\mathbf{q}}{(2\pi)^3} \int_0^{\bar{k}_F} e^{-i\mathbf{q}' \cdot \mathbf{R}} \frac{d\mathbf{q}'}{(2\pi)^3} \quad (\text{A2})$$

$$= -\bar{f} \left| \frac{\bar{k}_F^3}{6\pi^2} g(\bar{k}_F R) \right|^2 \equiv -\Pi_x^{\text{cofe}} N(\bar{k}_F R) \quad (\text{A3})$$

where $\Pi_x = -\frac{n^2}{\bar{f}}$, $g(x) = 3[\sin(x) - x \cos(x)]/x^3$ and $N(x) = |g(x)|^2$. Thus, we obtain eq. (27).

Appendix B: Hartree properties of coe HEGs

Let us consider eqs (17) and (18) for the special case of an HEG. First, we note that, $n_{\kappa\kappa} = n$ for every state and therefore, $n_{2,H} = n^2 + \Delta n_{2,H}$ where $\Delta n_{2,H}(\mathbf{r}, \mathbf{r}') = \sum_{\kappa \neq \kappa'} w_{\max(\kappa, \kappa')} n_{\kappa\kappa'}(\mathbf{r}) n_{\kappa'\kappa}(\mathbf{r}')$. Furthermore, the resulting pair-density can depend only on $\mathbf{R} = \mathbf{r} - \mathbf{r}'$ while symmetry means it depends only on $R = |\mathbf{r} - \mathbf{r}'|$. Thus,

$$\Delta \epsilon_H = \frac{1}{N} \Delta E_H = \frac{1}{n} \int \Delta n_{2,H}(R) \frac{4\pi R^2 dR}{2R} \quad (\text{B1})$$

where we used n^2 to cancel the background charge, $N = nV$ to cancel the integral over \mathbf{r} , and symmetry to simplify the remaining integral over $\mathbf{r}' = \mathbf{r} + \mathbf{R}$. Our goal is therefore to determine $\Delta n_{2,H}(R)$. Note, the working in this appendix is rather involved, so we will often drop superscripts w in working.

We are now ready to look at HEG ensembles. Consider a finite HEG of N electrons in a volume V , with density $n = N/V$. The orbitals are $\phi_{\mathbf{q}} \approx \frac{1}{\sqrt{V}} e^{i\mathbf{q} \cdot \mathbf{r}}$ for \mathbf{q} on an appropriate reciprocal space grid. Each state, $|\kappa\rangle$ has density $n_{s,\kappa\kappa}(\mathbf{r}) = N/V = n$. The ground state is $|0\rangle = |q_1^2 \cdots q_{N/2}^2\rangle$ and is unpolarized. Other states may be described using $|\kappa\rangle = \hat{P}_{\mathbf{Q}_{\kappa}} |0\rangle$ where \hat{P} promotes Fock orbitals in the Slater determinant and $\mathbf{Q}_{\kappa} := \begin{smallmatrix} q_{a_1} \cdots q_{a_p} \\ q_{i_1} \cdots q_{i_p} \end{smallmatrix}$ contains lists of from ($i \leq N/2$) and to ($a > N/2$) orbitals, including spin. Cross-densities, when $\kappa \neq \kappa'$, are $n_{s,\kappa\kappa'}(\mathbf{r}) = e^{i\Delta \mathbf{q}_{\kappa\kappa'} \cdot \mathbf{r}}/V$ or zero. The former result occurs if and only if \mathbf{Q}_{κ} and $\mathbf{Q}_{\kappa'}$ differ by a single orbital

of the same spin, giving $\Delta \mathbf{q}_{\kappa\kappa'} = \mathbf{q}_{\in \kappa} - \mathbf{q}_{\in \kappa'}$. We use “connected” (con) to refer to any pair of states κ and κ' that differ only by a single orbital, and call $\Delta \mathbf{q}_{\kappa\kappa'}$ the connection wavenumber.

Let us now consider the case that N electrons are assigned to $N/2 \leq M \leq N$ orbitals, for a mean occupation of $f = \frac{N}{M}$. There are $\mathcal{N}_T = \binom{2M}{N}$ total states once spin is accounted for, each of which is weighted by, $w = \frac{1}{\mathcal{N}_T}$. Each of the \mathcal{N}_T states, $|\kappa\rangle$, has $N_{\uparrow, \downarrow, \kappa}$ electrons of each spin, giving $\zeta_{\kappa} = \frac{N_{\uparrow, \kappa} - N_{\downarrow, \kappa}}{N}$. State $|\kappa\rangle$ is connected to C_{κ} other states. Since only one orbital may change at a time, we obtain $C_{\kappa} = N_{\uparrow, \kappa}(M - N_{\uparrow, \kappa}) + N_{\downarrow, \kappa}(M - N_{\downarrow, \kappa}) = NM - \frac{N^2}{2}(1 + \zeta_{\kappa}^2)$, where $N_{\uparrow, \downarrow, \kappa} \leq M$.

Our goal is to obtain useful properties of the Hartree pair-density. The pair-density is defined by,

$$\Delta n_{2,H}(\mathbf{R}) = \frac{1}{\mathcal{N}_T} \sum_{\kappa, \kappa' \text{ con } \kappa} \frac{e^{i\Delta \mathbf{q}_{\kappa\kappa'} \cdot \mathbf{R}}}{V^2}, \quad (\text{B2})$$

where we used $w_{\kappa} = w_{\kappa'} = \frac{1}{\mathcal{N}_T}$ and $\mathbf{r} - \mathbf{r}' := \mathbf{R}$. The special case of $\mathbf{r} = \mathbf{r}'$ ($\mathbf{R} = \mathbf{0}$) yields the “on-top” pair density deviation, $\Pi_H = \Delta n_{2,H}(\mathbf{R} = \mathbf{0})$, which is relatively straightforward to evaluate using, $\Delta n_{2,H} = \frac{1}{\mathcal{N}_T V^2} \sum_{\kappa} C_{\kappa}$, which follows from $e^{i\Delta \mathbf{q} \cdot \mathbf{R}} = 1$ for all connected states, and the definition of C_{κ} . Using C_{κ} from the above paragraph yields,

$$\Delta \Pi_H = \frac{1}{V^2} [NM + \frac{N^2}{2}(1 + \bar{\zeta}^2)] = n^2 \left[\frac{1}{f} - \frac{1 + \bar{\zeta}^2}{2} \right]. \quad (\text{B3})$$

where $\bar{\zeta}^2 = \frac{1}{\mathcal{N}_T} \sum_{\kappa} \zeta_{\kappa}^2$ is the ensemble averaged of the squared spin-polarization.

As an initial test, consider the above analysis for the two special types of gases, unpolarized and fully polarized gases, which have no ensemble effects and which must therefore yield $\Delta \Pi_H = 0$. An unpolarized gas involves $M = N/2$, $\bar{f} = 2$, $\mathcal{N}_T = 1$ and $\zeta_{\kappa} = 0$, yielding $\Delta \Pi_H = n^2(\frac{1}{2} - \frac{1}{2}) = 0$. A fully polarized gas involves $M = N$, $\bar{f} = 1$, $\mathcal{N}_T = 1$ and $\zeta_{\kappa} = 1$, yielding $\Delta \Pi_H = n^2(\frac{1}{1} - 1) = 0$. Thus, both exhibit the expected behaviour. We therefore see that eq. (B3) is consistent with existing results.

We are now ready to generalize to constant occupation factor (cof) gases, with $f_q = \bar{f} \Theta(\bar{k}_F - q)$, for $1 < \bar{f} < 2$. As discussed in the main text, we restricted to the special case of maximally polarized states, $|\kappa\rangle$, in which each state has the maximum spin-polarization allowed by \bar{f} . All these states involve $N_{\uparrow} = M$ and $N_{\downarrow} = N - M$ giving, $\zeta_{\kappa} = \frac{2M - N}{N} = \frac{2}{\bar{f}} - 1 = \bar{\zeta}$. Eq. (B3) then yields,

$$\Delta \Pi_H = n^2 \frac{(2 - \bar{f})(\bar{f} - 1)}{\bar{f}^2}, \quad \Pi_H = n^2 \frac{3\bar{f} - 2}{\bar{f}^2}. \quad (\text{B4})$$

for the on-top, $\mathbf{R} = \mathbf{0}$, pair-density.

We are now ready to move on from the on-top hole to consider general $\mathbf{R} \neq \mathbf{0}$. We first recognise that equal weighting of states is equivalent to equal weighting of con-

nection wavenumbers, yielding,

$$\begin{aligned}\Delta n_{2,H}(\mathbf{R}) &= \Delta \Pi_H \frac{1}{M^2} \sum_{\mathbf{q}} \sum_{\mathbf{q}' \neq \mathbf{q}} e^{i(\mathbf{q}-\mathbf{q}') \cdot \mathbf{R}} \\ &= \Delta \Pi_H \left[|g(\bar{k}_F R)|^2 - \frac{1}{M} \right],\end{aligned}\quad (\text{B5})$$

where $g := \frac{1}{M} \sum_{\mathbf{q}} e^{i\mathbf{q} \cdot \mathbf{R}}$. We next impose symmetry on the wavenumbers, and approximate the sum by an integral to obtain,

$$\begin{aligned}g(\bar{k}_F R) &\approx \frac{1}{M} \int_0^{(\frac{3M}{4\pi})^{1/3}} \frac{\sin(qk_V R)}{qk_V R} 4\pi q^2 dq \\ &= \frac{3[\sin(\bar{k}_F R) - \bar{k}_F R \cos(\bar{k}_F R)]}{(\bar{k}_F R)^3}\end{aligned}\quad (\text{B6})$$

where $k_V = 2\pi/V^{1/3}$ is the wavenumber associated with the volume V ; and $\bar{k}_F = (6\pi^2 M/V)^{1/3} = (6\pi^2 n/\bar{f})^{1/3}$ is the usual Fermi wavenumber. $g(x)$ the same expression found in eq. (A3). Note, $\Delta n_{2,H}(R)$ integrates to zero, as expected.

Finally, eq. (B1) becomes $\Delta \epsilon_H = \frac{\Delta \Pi_H}{n} [\int_0^\infty \frac{g(\bar{k}_F R)^2}{R} 2\pi R^2 dR - \frac{\bar{f}}{2n} (\frac{9\pi}{2V})^{1/3}]$. In the limit $V \rightarrow \infty$ the second term vanishes, yielding,

$$\Delta \epsilon_H^{\text{cofe}} = \bar{f} \Delta \Pi_H |\epsilon_x^{\text{cofe}}(r_s, \bar{f})| = \frac{C_H}{r_s} \frac{(2 - \bar{f})(\bar{f} - 1)}{\bar{f}^{4/3}} \quad (\text{B7})$$

$$= |\epsilon_x^{\text{cofe}}(r_s, \bar{f})| \frac{(2 - \bar{f})(\bar{f} - 1)}{\bar{f}} \quad (\text{B8})$$

where we used, $\epsilon_x^{\text{cofe}} = -\frac{\bar{f}}{n} \int_0^\infty \frac{g(\bar{k}_F R)^2}{R} 2\pi R^2 dR$ [which follows from $n_{2,x}(R) = -\bar{f} g(\bar{k}_F R)^2$] and $\epsilon_x^{\text{cofe}} = -\frac{C_x}{r_s} [2/\bar{f}]^{1/3}$ derived in the main text, to obtain $C_H = 2^{1/3} C_x = 0.577252$. Similarly,

$$n_{2,H}(R) = n^2 + \Delta n_{2,H}(R) = n^2 + \Delta \Pi_H^{\text{cofe}} N(\bar{k}_F R) \quad (\text{B9})$$

where $\Delta \Pi_H^{\text{cofe}}$ is defined in eq. (B4); and $N(x) = g(x)^2 = 9[\sin(x) - x \cos(x)]^2/x^6$ is the unitless function defined near eq. (27) or (A3).

Appendix C: State-driven correlation of cofe HEGs

1. State-driven correlation energy from the random-phase approximation

The state-driven correlation energy [eq. (39)] involves the response function at imaginary frequencies. The imaginary frequency density-density response of an unpolarized HEG is,

$$\chi_0(q, i\omega; r_s) := -\frac{k_F}{4\pi^2} C\left(\frac{q}{2k_F}, \frac{\omega}{qk_F}\right) \quad (\text{C1})$$

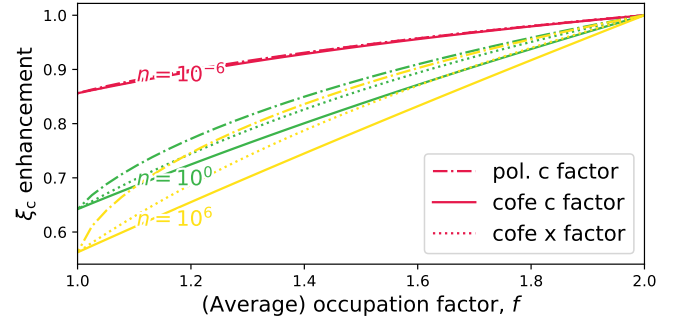


FIG. 7. Correlation enhancement of spin-polarized (dash-dot lines) and cofe (solid lines) HEGs as a function of occupation factor, f . The cofe to exchange factor (dotted lines) is also shown after rescaling to yield the same values for $\bar{f} = 1$ and $\bar{f} = 2$.

where $k_F = 1.9191583/r_s = (3\pi^2 n)^{1/3}$ is the Fermi wavenumber of an unpolarized gas. Here,

$$\begin{aligned}C(Q, \Gamma) &= 1 + \frac{\Gamma^2 - Q_+ Q_-}{4Q} \log \frac{Q_+^2 + \Gamma^2}{Q_-^2 + \Gamma^2} \\ &\quad + \Gamma \left[\tan^{-1} \frac{Q_-}{\Gamma} - \tan^{-1} \frac{Q_+}{\Gamma} \right]\end{aligned}\quad (\text{C2})$$

where $Q_\pm = Q \pm 1$. For brevity we shall use $Q = \frac{q}{2k_F}$ and $\Gamma = \frac{\omega}{qk_F}$ to always mean unpolarized gas quantities.

For a polarized HEG we take half of two unpolarized systems with $k_{F\uparrow} = k_F(1 + \zeta)^{1/3} := k_F h_+$ and $k_{F\downarrow} = k_F(1 - \zeta)^{1/3} := k_F h_-$. Therefore,

$$\chi_0(q, \omega; r_s, \zeta) = -\frac{k_F}{8\pi^2} \left[h_+ C\left(\frac{Q}{h_+}, \frac{\Gamma}{h_+}\right) + h_- C\left(\frac{Q}{h_-}, \frac{\Gamma}{h_-}\right) \right] \quad (\text{C3})$$

The cofe case of constant \bar{f} is easily dealt with by including a prefactor of \bar{f} on χ_0 , and using the cofe Fermi level, $k_F = k_F(2/\bar{f})^{1/3} := k_F g$. It follows from $\bar{f} = 2/g^3$ that,

$$\chi_0^{\text{cofe}}(q, \omega; r_s, \bar{f}) = -\frac{k_F}{4\pi^2 g^2} C\left(\frac{Q}{g}, \frac{\Gamma}{g}\right). \quad (\text{C4})$$

Setting $\zeta = 0$ and $\bar{f} = 2$ yields $h_\pm = g = 1$ and yields the same response as the unpolarized gas. Similarly, setting $\zeta = 1$ in (C3) gives the same result as setting $\bar{f} = 1$ in (C4), as expected.

From the response function we are able to evaluate the random-phase approximation for the correlation energy, via,

$$\epsilon_c^{\text{RPA}} = \frac{1}{2n} \int_0^\infty \frac{d\omega}{\pi} \int_0^\infty \frac{q^2 dq}{2\pi^2} \left[\chi_0 \frac{4\pi}{q^2} + \log(1 - \chi_0 \frac{4\pi}{q^2}) \right]. \quad (\text{C5})$$

This may be made more convenient by using $n = \frac{k_F^3}{3\pi^2}$, $q = 2k_F Q$ and $\omega = qk_F \Gamma$ to write,

$$\epsilon_c^{\text{RPA}} = \frac{12k_F^2}{\pi} I_{Q\Gamma} \left[\frac{\pi}{k_F^2 Q^2} \chi_0 \right]. \quad (\text{C6})$$

where $I_{QR}[f] := \int_0^\infty d\Gamma \int_0^\infty Q^3 dQ [-f + \log(1+f)]$. We may also define, $\bar{I}(P) = I_{QR} \left[\frac{P}{Q^2} C(Q, \Gamma) \right]$.

Thus, the RPA enhancement factor for a polarized, relative to an unpolarized gas at the same density, gas is,

$$\begin{aligned} \xi_c^{\text{RPA}}(\zeta) &= \frac{I_{QR} \left[\frac{Ph_+}{2Q^2} C\left(\frac{Q}{h_+}, \frac{\Gamma}{h_+}\right) + \frac{Ph_-}{2Q^2} C\left(\frac{Q}{h_-}, \frac{\Gamma}{h_-}\right) \right]}{I_{QR} \left[\frac{P}{Q^2} C(Q, \Gamma) \right]} \\ &= \frac{h_+^5 \bar{I}\left(\frac{P}{2h_+}\right) + h_-^5 \bar{I}\left(\frac{P}{2h_-}\right)}{\bar{I}(P)} \end{aligned} \quad (\text{C7})$$

where $h_\pm = (1 \pm \zeta)^{1/3}$. The equivalent enhancement factor of a cof ensemble HEG may be written as,

$$\xi_c^{\text{RPA,cofe}}(\bar{f}) = \frac{I_{QR} \left[\frac{P}{g^2 Q^2} C\left(\frac{Q}{g}, \frac{\Gamma}{g}\right) \right]}{I_{QR} \left[\frac{P}{Q^2} C(Q, \Gamma) \right]} = \frac{g^5 \bar{I}\left(\frac{P}{g^4}\right)}{\bar{I}(P)} \quad (\text{C8})$$

where $P := \frac{1}{2\pi k_F} = 0.08293r_s$ and $g = (2/\bar{f})^{1/3}$.

The RPA enhancement is expected to be accurate in the high-density of matter $k_F \rightarrow \infty$. Figure 7 shows (state-driven) correlation energy enhancement factors, $\xi_c^{\text{RPA}}(\zeta)$ and $\xi_c^{\text{RPA,cofe}}(f)$ as a function of the (average) occupation factor, \bar{f} , using $\zeta = \hat{f}_{x\text{-map}}^{-1}(\bar{f})$ [from eq. (D8)] for the effective spin-polarization. It reports ξ for high ($n = 10^6$), medium ($n = 1$) and low ($n = 10^{-6}$) densities. We see that the state-driven correlation energy of cofe HEGs is: i) virtually linear in \bar{f} , for high densities; ii) very similar to the (renormalized) on-top exchange enhancement factor, for low densities.

The high density ($r_s \rightarrow 0$) behaviour of ξ_c^{cofe} can be shown analytically, because $P \rightarrow 0$. We may therefore Taylor expand the log to obtain,

$$\lim_{r_s \rightarrow \infty} \bar{I}(P) \approx \int_0^\infty Q^3 dQ \int_0^\infty d\Gamma \frac{1}{2} \left(\frac{P}{Q^2} C \right)^2, \quad (\text{C9})$$

from which it follows that $\xi_c^{\text{cofe}} = g^5 \bar{I}(P/g^4)/\bar{I}(P) = g^5 (\frac{1}{g^4})^2 = g^{-3} = \bar{f}/2$ is linear in \bar{f} . The RPA is not appropriate for the low density limit, although we shall later see it is qualitatively correct.

2. State-driven correlation energies in general

We are now ready to use what we have learned about correlation energies from the RPA and theoretical arguments to obtain general expressions for the SD correlation energies in cofe HEGs. Let us begin with the low-density limit. The main text has shown that,

$$\lim_{r_s \rightarrow \infty} \epsilon_c^{\text{cofe}}(r_s, \bar{f}) = \epsilon_x(r_s) \left[\frac{C_\infty}{C_x} - f_{\text{Hx}}^{\text{cofe}}(\bar{f}) \right]. \quad (\text{C10})$$

It can also be shown that $\lim_{r_s \rightarrow \infty} \epsilon_c^{\text{DD,cofe}}(r_s, \bar{f}) \rightarrow -\Delta \epsilon_{\text{H}}^{\text{cofe}}(r_s, \bar{f})$ – this result is a specialized case of a broader relationship to be discussed in a future work.

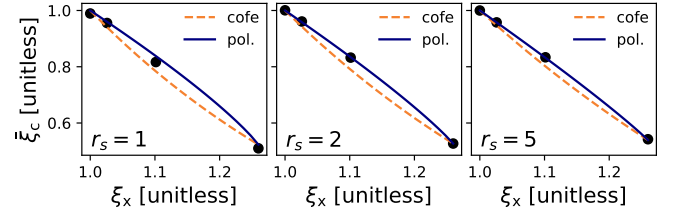


FIG. 8. $\bar{\xi}_c$ versus ξ_x using RPA data for cofe HEG (orange, dashed lines) and polarized HEG (navy, solid lines). Black dots indicate data from Ref. 8.

It is thus clear that the SD enhancement factor must capture the low-density scaling and cancel exchange:

$$\lim_{r_s \rightarrow \infty} \epsilon_c^{\text{SD,cofe}}(r_s, \bar{f}) \rightarrow \epsilon_x(r_s) \left[\frac{C_\infty}{C_x} - f_x^{\text{cofe}}(\bar{f}) \right]. \quad (\text{C11})$$

Surprisingly, this is consistent with the low-density behaviour shown in Figure 7 and so reveals that the RPA is qualitatively correct even in the low-density limit.

In the high-density limit, we instead obtain,

$$\begin{aligned} \lim_{r_s \rightarrow 0} \epsilon_c^{\text{SD,cofe}}(r_s, \bar{f}) &\rightarrow (\bar{f} - 1) \epsilon_c^U + (2 - \bar{f}) \epsilon_c^P \\ &= \epsilon_c^U + (2 - \bar{f}) [\epsilon_c^P - \epsilon_c^U] \end{aligned} \quad (\text{C12})$$

where $\epsilon_c^U := \epsilon_c(r_s, 0)$ is the correlation energy of an unpolarized gas and $\epsilon_c^P := \epsilon_c(r_s, 1)$ is the correlation energy of a fully polarized gas and $2 - \bar{f} = [\xi^{\text{RPA,cofe}}(\bar{f}) - \xi^{\text{RPA}}(0)]/[\xi^{\text{RPA}}(1) - \xi^{\text{RPA}}(0)]$. This is analogous to the known result that,

$$\lim_{r_s \rightarrow 0} \epsilon_c(r_s, \zeta) \rightarrow \epsilon_c^U + H^{\text{RPA}}(\zeta) [\epsilon_c^P - \epsilon_c^U], \quad (\text{C13})$$

where $H^{\text{RPA}}(\zeta) = -2[I(\zeta) - 1]$ is obtained from eq. (32) of Ref. 70 or, equivalently, $H^{\text{RPA}}(\zeta) := [\xi^{\text{RPA}}(\zeta) - \xi^{\text{RPA}}(0)]/[\xi^{\text{RPA}}(1) - \xi^{\text{RPA}}(0)]$. We cannot say anything about the DD correlation energy in this limit.

We thus obtain limiting behaviours for high and low-density HEGs. In typical polarized gases, one uses expansion in both limits together with QMC data, $\epsilon_c^{\text{QMC}}(r_s, \zeta)$, to fill in the gaps for moderate and large densities. We do not have QMC data for cofe gases. Thus, the final step in our analysis of correlation energies is to show how to reuse existing polarized gas QMC data for cofe HEGs.

As a first step, we assume that the high-density relationship [eq. (C13)] between RPA and exact results is true for moderate and large r_s . That is, we expect

$$\bar{\xi}_c := 1 + \frac{\xi_c(\zeta = 1) - 1}{\xi_c^{\text{RPA}}(\zeta = 1) - 1} [\xi_c^{\text{RPA}} - 1] \approx \xi_c^{\text{QMC}} \quad (\text{C14})$$

to be approximately valid for all r_s . The usefulness of this approximation is further supported by Figure 7, which shows that the RPA yields an approximately linear dependence on \bar{f} even for low-density HEGs where the RPA is expected to be poor.

The second step is to recognise that, in low-density gases, we may write, $\xi_c = \frac{C_\infty}{C_x} - \xi_x$ and $\xi_c^{\text{SD,cofe}} = \frac{C_\infty}{C_x} +$

ξ_x^{cofe} and therefore $\epsilon_c^{\text{SD,cofe}}(r_s \rightarrow 0, \bar{f}) \approx X(\epsilon_x^{\text{cofe}}(r_s, \bar{f}))$ where $\epsilon_c(r_s \rightarrow 0, \zeta) := X(\epsilon_x(r_s, \zeta))$ – here X is a single-variable function. Figure 8 shows that a similar result nearly holds for moderate r_s and, furthermore, that models of both cofe and polarized gases agree rather well with QMC data from Spink *et al* [8], despite the data being for polarized gases. We therefore assume that,

$$\epsilon_c^{\text{SD,cofe}}(r_s, \hat{f}_{\text{x-map}}(\zeta)) \approx \epsilon_c^{\text{QMC}}(r_s, \zeta) \quad (\text{C15})$$

for moderate and large densities with viable QMC data, where $\hat{f}_{\text{x-map}}$ is defined such that $\epsilon_x(\zeta) = \epsilon_x^{\text{cofe}}(\bar{f} = \hat{f}_{\text{x-map}}(\zeta))$. This is a rather good approximation in practice as the maximum difference between $\epsilon_c^{\text{SD,cofe}}$ using RPA and $\epsilon_c^{\text{SD,cofe}}$ using (C15) is 1 mHa for $r_s = 1$, and is sub-mHa for larger r_s .

Thus, equations (C12), (C15) and (C11) provide a set of constraints and reference values (from existing QMC data) for high, moderate and low densities, respectively. These three relationships are used in Appendix D to produce the parametrisation for the state-driven correlation energy of a cofe HEG.

Note, it would be very desirable to obtain QMC or similar-quality reference data for cofe HEGs, to provide direct inputs for parametrisations. The derivative, $de^{\text{cofe}}(r_s, \bar{f})/d\bar{f}|_{\bar{f}=2}$, may be amenable to computation using existing techniques, as it involves only low-lying excited states.

Appendix D: Parameterizations

The main text and previous appendices have introduced five terms that go into the cofe HEG energy as a function of r_s and \bar{f} . This appendix will provide a useful parametrisation of the state-driven (SD) correlation energy that will allow the use of cofe HEGs in density functional approximations. As explained in the main text, the cofe-based LDA should be,

$$E_{\text{xc}}^{\text{cofeLDA}} := \int n(\mathbf{r})[\epsilon_x(r_s)f_x^{\text{cofe}}(\bar{f}) + \epsilon_c^{\text{SD,cofe}}(r_s, \bar{f})], \quad (\text{D1})$$

where $r_s(\mathbf{r})$ and $\bar{f}(\mathbf{r})$ depend on local properties of the inhomogeneous system.

The exchange term involves the closed form expression of eq. (26). The correlation term, $\epsilon_c^{\text{SD,cofe}}(r_s, \bar{f})$, needs to be parametrised using:

1. The known high-density behaviour of eq. (40);
2. The known low-density behaviour of eq. (41).
3. QMC data for other densities, adapted using eq. (42);

The high-density limit yields, [to $O(r_s \log(r_s))$]

$$\epsilon_c^{\text{SD,cofe}}(r_s \rightarrow 0, \bar{f}) := c_0(\bar{f}) \log r_s - c_1(\bar{f}) \quad (\text{D2})$$

TABLE II. Correlation energy parameters for selected values of ζ from fits to benchmark data [8] and exact constraints.

ζ^{QMC}	A	α	β_1	β_2	β_3	β_4
cofe parameters						
0.00	0.031091	0.1825	7.5961	3.5879	1.2666	0.4169
0.34	0.028833	0.2249	8.1444	3.8250	1.6479	0.5279
0.66	0.023303	0.2946	9.8903	4.5590	2.5564	0.7525
1.00	0.015545	0.1260	14.1229	6.2011	1.6503	0.3954
rPW92 parameters						
0.00	0.031091	0.1825	7.5961	3.5879	1.2666	0.4169
0.34	0.030096	0.1842	7.9233	3.7787	1.3510	0.4326
0.66	0.026817	0.1804	9.0910	4.4326	1.5671	0.4610
1.00	0.015546	0.1259	14.1225	6.2009	1.6496	0.3952

where the parameters $c_{0,1}(\bar{f})$ are linear in \bar{f} and are trivially related to their un- and fully-polarized counterparts. [10] The low-density limit yields, [to $O(\frac{1}{r_s^2})$]

$$\epsilon_c^{\text{SD,cofe}}(r_s \rightarrow \infty, \bar{f}) := \frac{-C_\infty + C_x[2/\bar{f}]^{1/3}}{r_s} + \frac{C'_\infty}{r_s^{3/2}}. \quad (\text{D3})$$

where C_∞ , C_x and C'_∞ are universal parameters that do not depend on \bar{f} . [47]

Perdew and Wang [10] proposed that HEG correlation energies lend themselves to a parameterization,

$$F(r_s; P) := -2A(1 + \alpha r_s) \log \left[1 + \frac{1}{2A \sum_{i=1}^4 \beta_i r_s^{i/2}} \right] \quad (\text{D4})$$

where $P = (A, \alpha, \beta_1, \beta_2, \beta_3, \beta_4)$ is a set of parameters that depend on ζ , \bar{f} or related variables. By construction, eq. (D4) can be made exact to leading orders for small and large r_s . The high-density limit yields,

$$A^{\text{cofe}} = c_0, \quad \beta_1^{\text{cofe}} = \frac{e^{-c_1/(2c_0)}}{2c_0}, \quad \beta_2^{\text{cofe}} = 2A\beta_1^2, \quad (\text{D5})$$

where the coefficients are,

$$c_0(\bar{f}) = \frac{0.031091\bar{f}}{2}, \quad c_1(\bar{f}) = 0.00454 + \frac{0.0421\bar{f}}{2}.$$

The low-density limit yields,

$$\beta_4^{\text{cofe}} = \frac{\alpha}{C_\infty - C_x f_x^{\text{cofe}}(\bar{f})}, \quad \beta_3^{\text{cofe}} = \frac{\beta_4^2 C'_\infty}{\alpha}, \quad (\text{D6})$$

using the parameters $C_\infty \approx 1.95C_x$ and $C'_\infty = 1.33$ [71] from Sec. IIIC, and $f_x^{\text{cofe}}(\bar{f}) = [2/\bar{f}]^{1/3}$ from eq. (26). Thus, only α is left undefined.

Our goal is to find parameters, $P(\bar{f})$, that can be used in a constant occupation factor (cof) parameterization, $\epsilon_c^{\text{cofe}}(r_s, \bar{f}^*) := F(r_s; P^{\text{cofe}}(\bar{f}^*))$, of the cofe HEG at selected values of \bar{f}^* ; and interpolated to general \bar{f} . Our first step is to pick the values of \bar{f}^* . We seek to adapt the high-quality QMC data of Spink *et al* [8], who

TABLE III. Weighted sum parameters for $M_{2,3}$ (Appendix D) and $Z_{2,3}$ (Appendix E). E.g., $M_2 = -2\epsilon_c^0 + 4\epsilon_c^{0.66} - 2\epsilon_c^1$ and $Z_3 = 19.86\epsilon_c^0 - 30.57\epsilon_c^{0.34} + 12.71\epsilon_c^{0.66} - 2\epsilon_c^1$.

Function	ϵ_c^0	$\epsilon_c^{0.34}$	$\epsilon_c^{0.66}$	ϵ_c^1
cofe parameters				
M_2	-2.00	0.00	4.00	-2.00
M_3	13.33	-22.41	11.43	-2.35
rPW92 parameters				
Z_2	-10.95	13.32	-1.47	-0.90
Z_3	19.86	-30.57	12.71	-2.00

provided correlation energies for, $\zeta^* \in (0, 0.34, 0.66, 1)$, using eq. (42). We therefore seek parametrizations at $\bar{f}^* = \hat{f}_{x\text{-map}}^{-1}(\zeta^*)$, so that the right-hand side of eq. (42) is known.

As a first step, we must find $\hat{f}_{x\text{-map}}$ and its inverse. Setting eqs. (5) and (26) to be equal yields,

$$\hat{f}_{x\text{-map}}(\zeta) \approx 2 - \frac{4}{3}\zeta^2 + \frac{1}{6}[1.0187\zeta^3 + 0.9813\zeta^4], \quad (\text{D7})$$

$$\hat{f}_{x\text{-map}}^{-1}(\bar{f}) \approx \sqrt{\frac{3}{4}(2 - \bar{f})} [1 + (\sqrt{\frac{4}{3}} - 1)(2 - \bar{f})], \quad (\text{D8})$$

which are exact in the polarized and unpolarized limits, and accurate to within 0.2% for all ζ and \bar{f} . Eq. (D7) gives $\bar{f}^* \in (2, 1.85, 1.50, 1)$ for $\zeta^* \in (0, 0.34, 0.66, 1)$, which are the \bar{f} values we use in fits. Then, for each \bar{f}^* , we obtain $\alpha(\bar{f}^*)$ by minimizing,

$$\min_{\alpha} \sum_{r_s \in \text{QMC}} |\epsilon_{c,\text{QMC}}^{\zeta^{\text{QMC}}}(r_s) - \epsilon_c^{\text{SD,cofe}}(r_s, \bar{f}^*)| \quad (\text{D9})$$

where $\epsilon_{c,\text{QMC}}^{\zeta^{\text{QMC}}}(r_s)$ is correlation energy data from Ref. 8 and $\epsilon_c^{\text{SD,cofe}}(r_s, \bar{f}^*) := F(r_s, P(\bar{f}^*))$ involves the five constrained coefficients and free $\alpha(\bar{f}^*)$. Optimal parameters for the four values of ζ^* (called ζ^{QMC} to highlight their origin) are reported in Table II.

The next step of our parametrisation departs from PW92, in that we approximate the correlation energy at arbitrary \bar{f} via cubic fits (in \bar{f}) to the QMC data. Thus,

$$\epsilon_c^{\text{cofe}}(r_s, \bar{f}) := (\bar{f} - 1)\epsilon_c^0(r_s) + (2 - \bar{f})\epsilon_c^1(r_s) + (\bar{f} - 1)(2 - \bar{f})[M_2(r_s) + (\frac{3}{2} - \bar{f})M_3(r_s)], \quad (\text{D10})$$

where $\epsilon_c^{\zeta}(r_s) := F(r_s, P_{\zeta})$ is computed using eq. (D4) and M_2 and M_3 involve weighted sums of $\epsilon_c(r_s, \bar{f})$ at selected values of \bar{f} . This fit becomes exact in the high-density limit, as the correlation energy is linear in \bar{f} ; and is also extremely accurate in the low-density limit as $(2/\bar{f})^{1/3}$ for $\bar{f} \in [1, 2]$ may be reproduced to within 0.1% by a cubic fit. A cubic fit on $\bar{f}^* \in (2, 1.85, 1.50, 1)$ yields,

$$M_2(r_s) := 2[2\epsilon_c^{0.66}(r_s) - \epsilon_c^0(r_s) - \epsilon_c^1(r_s)], \quad (\text{D11})$$

$$M_3(r_s) := \frac{40}{357}[102\epsilon_c^{0.66}(r_s) - 200\epsilon_c^{0.34}(r_s) + 119\epsilon_c^1(r_s) - 21\epsilon_c^0(r_s)], \quad (\text{D12})$$

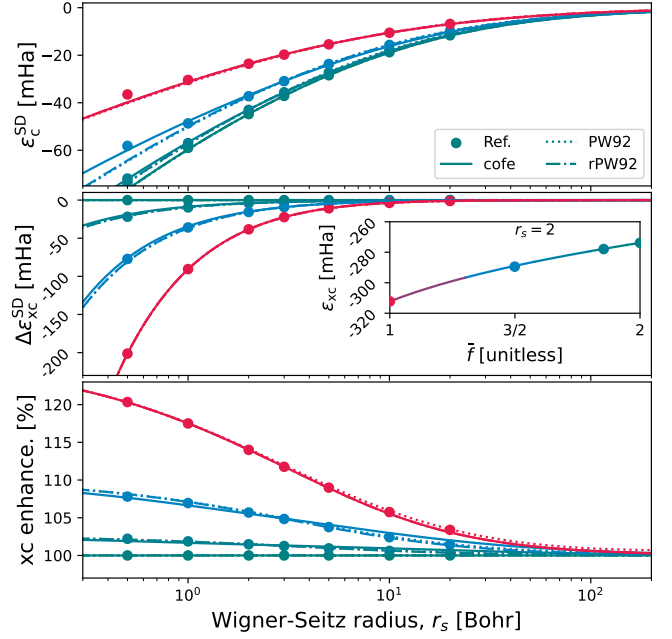


FIG. 9. Like Figure 3 but with the addition of polarized HEG results from PW92 [10] (dots) and rPW92 (dash-dot) for $\zeta \in (0, 0.34, 0.66, 1)$, to show differences between cofe and polarized gases in the high-density limit.

where α is optimized on each of the four spin-polarizations.

The same strategy may also be applied to a conventional spin-polarized HEG. Thus, in addition to parameters for the cofe model, Tables II and III also contains a set of coefficients for a “revised PW92” (rPW92) model that is an analogue of the cofe model introduced here. Details are provided in Appendix E. As it is based on similar principles, rPW92 is more directly comparable to the cofe parametrization provided here than the original PW92, especially in the low-density limit.

Appendix E: Revised PW92

The “revised PW92” (rPW92) parameterization is designed as a direct replacement for the original PW92 model. [10] Its main differences are: 1) the use of a cubic fit in ζ^2 , analogous to the fit to \bar{f} used in the main text; 2) the use of the most up-to-date understanding of the low density limit, per Sec. IIIC; and 3) α is found from the Spink reference data. [8] Note, we fit to ζ^2 because exchange and correlation are quadratic for $\zeta \rightarrow 0$, but linear for $\bar{f} \rightarrow 2$.

The revised PW92 (rPW92) parameterization of correlation energies is,

$$\epsilon_c^{\text{rPW92}}(r_s, \zeta) := (1 - \zeta^2)\epsilon_c^0 + \zeta^2\epsilon_c^1 + (1 - \zeta^2)\zeta^2[Z_2(r_s) + \zeta^2Z_3(r_s)]. \quad (\text{E1})$$

where coefficients for $Z_{2,3}$ are reported in Table III. Interestingly, the values we obtain for α at $\zeta = 0$ and $\zeta = 1$ are slightly lower than those from the original PW92 parametrisation, [10] most likely due to the use of more modern QMC data.

Figure 9 shows results from Figure 3 plus the LSDA (rPW92) parametrised along similar lines. It also includes results from an existing LSDA (PW92 [10]). By construction, both c0e and rPW92 do a better job

of capturing the SCE limit, especially as PW92 incorrectly yields different low-density behaviours for different ζ . It is important to recognise that differences (for $\zeta = 0.34$ and 0.66) between c0e enhancement factors and PW92/rPW92 *do not represent errors*, but rather represent different quantum physics captured by c0e and polarized gases, which lead to different high density behaviours.

-
- [1] P. Hohenberg and W. Kohn, Inhomogeneous electron gas, *Phys. Rev.* **136**, B864 (1964).
 - [2] W. Kohn and L. J. Sham, Self-consistent equations including exchange and correlation effects, *Phys. Rev.* **140**, A1133 (1965).
 - [3] L. H. Thomas, The calculation of atomic fields, *Math. Proc. Cambridge Philos. Soc.* **23** (1927).
 - [4] E. Fermi, Un metodo statistico per la determinazione di alcune proprieta dell'atomo, *Rend. Accad. Naz. Lincei* **6** (1927).
 - [5] AKA jellium or uniform electron gas – we shall use HEG exclusively throughout.
 - [6] D. M. Ceperley and B. J. Alder, Ground state of the electron gas by a stochastic method, *Phys Rev Lett* **45**, 566 (1980).
 - [7] F. H. Zong, C. Lin, and D. M. Ceperley, Spin polarization of the low-density three-dimensional electron gas, *Phys Rev E* **66**, 036703 (2002).
 - [8] G. G. Spink, R. J. Needs, and N. D. Drummond, Quantum monte carlo study of the three-dimensional spin-polarized homogeneous electron gas, *Phys. Rev. B* **88**, 085121 (2013).
 - [9] S. H. Vosko, L. Wilk, and M. Nusair, Accurate spin-dependent electron liquid correlation energies for local spin density calculations: a critical analysis, *Can J Phys* **58**, 1200 (1980).
 - [10] J. P. Perdew and Y. Wang, Accurate and simple analytic representation of the electron-gas correlation energy, *Phys. Rev. B* **45**, 13244 (1992).
 - [11] T. Chachiyo, Communication: Simple and accurate uniform electron gas correlation energy for the full range of densities, *J. Chem. Phys.* **145**, 021101 (2016).
 - [12] E. H. Lieb, Thomas-Fermi and related theories of atoms and molecules, *Rev. Mod. Phys.* **53**, 603 (1981).
 - [13] P. Elliott, D. Lee, A. Cangi, and K. Burke, Semiclassical origins of density functionals, *Phys. Rev. Lett.* **100**, 256406 (2008).
 - [14] K. Burke, A. Cancio, T. Gould, and S. Pittalis, Locality of correlation in density functional theory, *J. Chem. Phys.* **145**, 10.1063/1.4959126 (2016).
 - [15] J. P. Perdew and K. Schmidt, Jacob's ladder of density functional approximations for the exchange-correlation energy, *AIP Conf. Proc.* **577**, 1 (2001).
 - [16] A. D. Becke, Density-functional exchange-energy approximation with correct asymptotic behavior, *Phys Rev A* **38**, 3098 (1988).
 - [17] J. P. Perdew, K. Burke, , and M. Ernzerhof, Generalized gradient approximation made simple, *Phys. Rev. Lett.* **77**, 3865 (1996).
 - [18] J. Sun, A. Ruzsinszky, and J. Perdew, Strongly constrained and appropriately normed semilocal density functional, *Phys Rev Lett* **115**, 036402 (2015).
 - [19] J.-D. Chai and M. Head-Gordon, Systematic optimization of long-range corrected hybrid density functionals, *J. Chem. Phys.* **128**, 084106 (2008).
 - [20] N. T. Maitra, F. Zhang, R. J. Cave, and K. Burke, Double excitations within time-dependent density functional theory linear response, *J. Chem. Phys.* **120**, 5932 (2004).
 - [21] N. T. Maitra, Undoing static correlation: Long-range charge transfer in time-dependent density-functional theory, *J. Chem. Phys.* **122**, 234104 (2005).
 - [22] H. Iikura, T. Tsuneda, T. Yanai, and K. Hirao, A long-range correction scheme for generalized-gradient-approximation exchange functionals, *J. Chem. Phys.* **115**, 3540 (2001).
 - [23] T. Stein, L. Kronik, and R. Baer, Reliable prediction of charge transfer excitations in molecular complexes using time-dependent density functional theory, *J Am Chem Soc* **131**, 2818 (2009).
 - [24] N. T. Maitra, Charge transfer in time-dependent density functional theory, *J. Phys.: Cond. Matter* **29**, 423001 (2017).
 - [25] P. de Silva, Inverted singlet–triplet gaps and their relevance to thermally activated delayed fluorescence, *J. Phys. Chem. Lett.* **10**, 5674 (2019).
 - [26] J. Ehrmaier, E. J. Rabe, S. R. Pristash, K. L. Corp, C. W. Schlenker, A. L. Sobolewski, and W. Domcke, Singlet–triplet inversion in heptazine and in polymeric carbon nitrides, *J. Phys. Chem. A* **123**, 8099 (2019).
 - [27] S. Ghosh and K. Bhattacharyya, Origin of the failure of density functional theories in predicting inverted singlet–triplet gaps, *J. Phys. Chem. A* **126**, 1378 (2022).
 - [28] E. K. U. Gross, L. N. Oliveira, and W. Kohn, Rayleigh-ritz variational principle for ensembles of fractionally occupied states, *Phys. Rev. A* **37**, 2805 (1988).
 - [29] E. K. U. Gross, L. N. Oliveira, and W. Kohn, Density-functional theory for ensembles of fractionally occupied states. i. basic formalism, *Phys. Rev. A* **37**, 2809 (1988).
 - [30] E. Pastorczyk and K. Pernal, Ensemble density variational methods with self- and ghost-interaction-corrected functionals, *J. Chem. Phys.* **140**, 18A514 (2014).
 - [31] M. Filatov, M. Huix-Rotlant, and I. Burghardt, Ensemble density functional theory method correctly describes bond dissociation, excited state electron transfer, and double excitations, *J. Chem. Phys.* **142**, 184104 (2015).
 - [32] M. Filatov, Ensemble DFT approach to excited states of strongly correlated molecular systems, in *Density-Functional Methods for Excited States*, edited by

- N. Ferré, M. Filatov, and M. Huix-Rotllant (Springer International Publishing, Cham, 2016) pp. 97–124.
- [33] A. Pribram-Jones, Z.-h. Yang, J. R. Trail, K. Burke, R. J. Needs, and C. A. Ullrich, Excitations and benchmark ensemble density functional theory for two electrons, *J. Chem. Phys.* **140** (2014).
- [34] Z.-h. Yang, J. R. Trail, A. Pribram-Jones, K. Burke, R. J. Needs, and C. A. Ullrich, Exact and approximate Kohn-Sham potentials in ensemble density-functional theory, *Phys. Rev. A* **90**, 042501 (2014).
- [35] Z.-h. Yang, A. Pribram-Jones, K. Burke, and C. A. Ullrich, Direct extraction of excitation energies from ensemble density-functional theory, *Phys. Rev. Lett.* **119**, 033003 (2017).
- [36] T. Gould, L. Kronik, and S. Pittalis, Charge transfer excitations from exact and approximate ensemble Kohn-Sham theory, *J. Chem. Phys.* **148**, 174101 (2018).
- [37] F. Sagredo and K. Burke, Accurate double excitations from ensemble density functional calculations, *J. Chem. Phys.* **149**, 134103 (2018).
- [38] K. Deur and E. Fromager, Ground and excited energy levels can be extracted exactly from a single ensemble density-functional theory calculation, *J. Chem. Phys.* **150**, 094106 (2019).
- [39] C. Marut, B. Senjean, E. Fromager, and P.-F. Loos, Weight dependence of local exchange-correlation functionals in ensemble density-functional theory: Double excitations in two-electron systems, *Faraday Discuss.* (2020).
- [40] T. Gould, Approximately Self-Consistent Ensemble Density Functional Theory With All Correlations, *J Phys Chem Lett* **11**, 9907 (2020).
- [41] T. Gould, L. Kronik, and S. Pittalis, Double excitations in molecules from ensemble density functionals: Theory and approximations, *Phys Rev A* **104**, 022803 (2021).
- [42] T. Gould, Z. Hashimi, L. Kronik, and S. G. Dale, Single excitation energies obtained from the ensemble “HOMO–LUMO gap”: Exact results and approximations, *The Journal of Physical Chemistry Letters* **13**, 2452 (2022).
- [43] T. Gould and S. Pittalis, Hartree and exchange in ensemble density functional theory: Avoiding the nonuniqueness disaster, *Phys. Rev. Lett.* **119**, 243001 (2017).
- [44] T. Gould and S. Pittalis, Density-driven correlations in many-electron ensembles: Theory and application for excited states, *Phys. Rev. Lett.* **123**, 016401 (2019).
- [45] E. Fromager, Individual correlations in ensemble density-functional theory: State-driven/density-driven decompositions without additional Kohn-Sham systems, *Phys. Rev. Lett.* **124**, 243001 (2020).
- [46] T. Gould, G. Stefanucci, and S. Pittalis, Ensemble density functional theory: Insight from the fluctuation-dissipation theorem, *Phys. Rev. Lett.* **125**, 233001 (2020).
- [47] T. Gould, D. P. Kooi, P. Gori-Giorgi, and S. Pittalis, Electronic excited states in extreme limits via ensemble density functionals, *Phys Rev Lett* **130**, 106401 (2023).
- [48] J. Kirkpatrick, B. McMorro, D. H. P. Turban, A. L. Gaunt, J. S. Spencer, A. G. D. G. Matthews, A. Obika, L. Thiry, M. Fortunato, D. Pfau, L. R. Castellanos, S. Petersen, A. W. R. Nelson, P. Kohli, P. Mori-Sánchez, D. Hassabis, and A. J. Cohen, Pushing the frontiers of density functionals by solving the fractional electron problem, *Science* **374**, 1385 (2021).
- [49] M. Levy, Universal variational functionals of electron densities, first-order density matrices, and natural spin-orbitals and solution of the v -representability problem, *Proc. Natl. Acad. Sci.* **76**, 6062 (1979).
- [50] E. H. Lieb, Density functionals for coulomb systems, *Int J Quantum Chem* **24**, 243 (1983).
- [51] U. von Barth and L. Hedin, A local exchange-correlation potential for the spin polarized case. i, *J. Phys. C: Solid State Phys.* **5**, 1629 (1972).
- [52] N. D. Mermin, Thermal properties of the inhomogeneous electron gas, *Phys Rev* **137**, A1441 (1965).
- [53] S. M. Valone, A one-to-one mapping between one-particle densities and some n -particle ensembles, *J. Chem. Phys.* **73**, 4653 (1980).
- [54] J. P. Perdew, R. G. Parr, M. Levy, and J. L. Balduz, Density-functional theory for fractional particle number: Derivative discontinuities of the energy, *Phys. Rev. Lett.* **49**, 1691 (1982).
- [55] B. Senjean and E. Fromager, Unified formulation of fundamental and optical gap problems in density-functional theory for ensembles, *Phys. Rev. A* **98**, 022513 (2018).
- [56] ‘cofe’ is pronounced like coffee by the authors.
- [57] E. Wigner, On the interaction of electrons in metals, *Phys Rev* **46**, 1002 (1934).
- [58] E. Wigner, Effects of the electron interaction on the energy levels of electrons in metals, *Trans. Faraday Soc.* **34**, 678 (1938).
- [59] S. Azadi and N. D. Drummond, Low-density phase diagram of the three-dimensional electron gas, *Phys Rev B* **105**, 245135 (2022).
- [60] E. Alves, G. L. Bendazzoli, S. Evangelisti, and J. A. Berger, Accurate ground-state energies of wigner crystals from a simple real-space approach, *Phys Rev B* **103**, 245125 (2021).
- [61] S. Śmiga, F. D. Sala, P. Gori-Giorgi, and E. Fabiano, Self-consistent implementation of kohn–sham adiabatic connection models with improved treatment of the strong-interaction limit, *J Chem Theory Comput* **18**, 5936 (2022).
- [62] See Supplementary Material, including Ref. 72.
- [63] R. M. Parrish, L. A. Burns, D. G. A. Smith, A. C. Simmonett, A. E. DePrince, E. G. Hohenstein, U. Bozkaya, A. Y. Sokolov, R. D. Remigio, R. M. Richard, J. F. Gonthier, A. M. James, H. R. McAlexander, A. Kumar, M. Saitow, X. Wang, B. P. Pritchard, P. Verma, H. F. Schaefer, K. Patkowski, R. A. King, E. F. Valeev, F. A. Evangelista, J. M. Turney, T. D. Crawford, and C. D. Sherrill, Psi4 1.1: An open-source electronic structure program emphasizing automation, advanced libraries, and interoperability, *J. Chem. Theory Comput.* **13**, 3185 (2017).
- [64] D. G. A. Smith, L. A. Burns, D. A. Sirianni, D. R. Nascimento, A. Kumar, A. M. James, J. B. Schriber, T. Zhang, B. Zhang, A. S. Abbott, E. J. Berquist, M. H. Lechner, L. A. Cunha, A. G. Heide, J. M. Waldrop, T. Y. Takeshita, A. Alenaizan, D. Neuhauser, R. A. King, A. C. Simmonett, J. M. Turney, H. F. Schaefer, F. A. Evangelista, A. E. DePrince, T. D. Crawford, K. Patkowski, and C. D. Sherrill, Psi4numpy: An interactive quantum chemistry programming environment for reference implementations and rapid development, *J. Chem. Theory Comput.* **14**, 3504 (2018).
- [65] Q. Sun, T. C. Berkelbach, N. S. Blunt, G. H. Booth,

- S. Guo, Z. Li, J. Liu, J. D. McClain, E. R. Sayfutyarova, S. Sharma, S. Wouters, and G. K. Chan, PySCF: the python-based simulations of chemistry framework, *WIREs Comput. Mol. Sci.* **8**, 10.1002/wcms.1340 (2017).
- [66] Q. Sun, X. Zhang, S. Banerjee, P. Bao, M. Barbry, N. S. Blunt, N. A. Bogdanov, G. H. Booth, J. Chen, Z.-H. Cui, J. J. Eriksen, Y. Gao, S. Guo, J. Hermann, M. R. Hermes, K. Koh, P. Koval, S. Lehtola, Z. Li, J. Liu, N. Mardirossian, J. D. McClain, M. Motta, B. Mussard, H. Q. Pham, A. Pulkin, W. Purwanto, P. J. Robinson, E. Ronca, E. R. Sayfutyarova, M. Scheurer, H. F. Schurkus, J. E. T. Smith, C. Sun, S.-N. Sun, S. Upadhyay, L. K. Wagner, X. Wang, A. White, J. D. Whitfield, M. J. Williamson, S. Wouters, J. Yang, J. M. Yu, T. Zhu, T. C. Berkelbach, S. Sharma, A. Y. Sokolov, and G. K.-L. Chan, Recent developments in the PySCF program package, *J. Chem. Phys.* **153**, 10.1063/5.0006074 (2020).
- [67] J. Lee, L. W. Bertels, D. W. Small, and M. Head-Gordon, Kohn-sham density functional theory with complex, spin-restricted orbitals: Accessing a new class of densities without the symmetry dilemma, *Physical Review Letters* **123**, 113001 (2019).
- [68] J. Lee and M. Head-Gordon, Two single-reference approaches to singlet biradicaloid problems: Complex, restricted orbitals and approximate spin-projection combined with regularized orbital-optimized möller-plesset perturbation theory, *The Journal of Chemical Physics* **150**, 10.1063/1.5097613 (2019).
- [69] M. Véril, A. Scemama, M. Caffarel, F. Lipparini, M. Boggio-Pasqua, D. Jacquemin, and P. Loos, Questdb: A database of highly accurate excitation energies for the electronic structure community, *WIREs Computational Molecular Science* **11**, 10.1002/wcms.1517 (2021).
- [70] Y. Wang and J. P. Perdew, Correlation hole of the spin-polarized electron gas, with exact small-wave-vector and high-density scaling, *Phys Rev B* **44**, 13298 (1991).
- [71] M. Seidl, S. Giarrusso, S. Vuckovic, E. Fabiano, and P. Gori-Giorgi, Communication: Strong-interaction limit of an adiabatic connection in hartree-fock theory, *J. Chem. Phys.* **149**, 241101 (2018).
- [72] G. Levi, A. V. Ivanov, and H. Jónsson, Variational calculations of excited states via direct optimization of the orbitals in dft, *Faraday Discuss.* **224**, 448 (2020).